

Theory of Cuprate Pseudogap as Antiferromagnetic Order with Domain Walls

R.S. Markiewicz and A. Bansil¹

¹ *Physics Department, Northeastern University, Boston MA 02115, USA*

While magnetic fields generally compete with superconductivity, a type II superconductor can persist to very high fields by confining the field in topological defects, namely vortices. We propose that a similar physics underlies the pseudogap phase in cuprates, where the relevant topological defects are the antiphase domain walls of an underlying antiferromagnetic (AFM) order. A key consequence of this scenario is that the termination of the pseudogap phase should be quantitatively described by the underlying AFM model. We demonstrate that this picture can explain a number of key experimentally observed signatures of the pseudogap phase and how it collapses in the cuprates.

PACS numbers:

I. INTRODUCTION

A major stumbling-block to understanding high- T_c superconductivity is the mysterious ‘normal-phases’ – the pseudogap and strange-metal phases – that give birth to superconductivity. Why, for instance do so many strongly-correlated materials display strong intermingling/competition among multiple phases, variously labelled as ‘intertwined’¹ or ‘vestigial’² orders? To what extent are these behaviors universal?

Here, we focus on the termination of the cuprate pseudogap, where recent experiments have given hints that this termination shares a number of characteristic traits among cuprates, and that these universal traits pose a strong challenge for the theory of the pseudogap. Reference 3 proposes five experimental signatures of pseudogap collapse at doping x_{pg} : (1) logarithmic specific heat divergence; (2) jump in hole doping from x to $1+x$; (3) T -linear resistivity extending to $T=0$ at x_{pg} ; (4) Wiedemann-Franz law holding on both sides of x_{pg} ; and (5) a thermal Hall effect with opposite sign from the electronic Hall effect. While features 3-5 are sensitive to the scattering processes, 1 and 2 are relatively insensitive, and we here demonstrate that a simple model of antiferromagnetic (AFM) short-range order collapse remarkably captures these signatures, if the role of the Van Hove singularities (VHSs) is appropriately taken into account.

The lack of long-range ordered phases, the presence of texture, and yet enough coherence to display a (nanoscale) Fermi surface⁴ are all suggestive of a system dominated by short-range order, with the competing phases associated with topological defects of that order. Notably, recent density functional theory calculations, using advanced exchange-correlation potentials that can capture the insulating phase in undoped cuprates, have found just such a picture for near-optimally doped $\text{YBa}_2\text{Cu}_3\text{O}_7$ (YBCO7).⁵ Nearly two dozen magnetic phases were found, most with comparable energy per planar Cu, organized such that the materials with higher magnetic moment systematically had lower energy. By analyzing the phases, all were found to consist of an underlying AFM order with regular arrays of topological defects – either stacking faults or (doped) domain walls – exactly what would be needed to explain the proposed pseudogap textures. A natural assumption, then, is that the pseudogap order is predominantly AFM, but in the absence of electronic single crystals, there is a need to average over granular domains. In such a case, the thermodynamic properties (signatures 1 and 2 above) would be dominated by the AFM, until the domains get too small.

In this case, a self-consistent calculation of the AFM collapse⁶ follows an evolution similar to that seen experimentally. The magnetization decreases approximately linearly with doping to a certain doping x_{pg} , then drops to zero discontinuously in a first-order transition. Moreover, the AFM stabilization energy is essentially controlled by the Van Hove singularity (VHS) of the lower magnetic band, so that the first-order transition occurs when this VHS crosses the Fermi level and the AFM becomes unstable.

Potential problems with this scenario were quickly pointed out: (1) the nonmagnetic VHS density of states (DOS) at doping x_{VHS} is logarithmic but too weak to explain the divergent heat capacity; and (2) if $x_{pg} = x_{VHS}$, then the large Fermi surface for $x > x_{VHS}$ should be electron-like with area $\sim 1-x$, rather than the observed hole-like with area $\sim 1+x$. In fact, we shall see that the role of VHS is quite complicated, with three distinct manifestations in angle-resolved photoemission spectroscopy (ARPES), neutron scattering, and Hall effect.

Below, we summarize our key results, leaving the technical details to the Supplementary Material (SM).

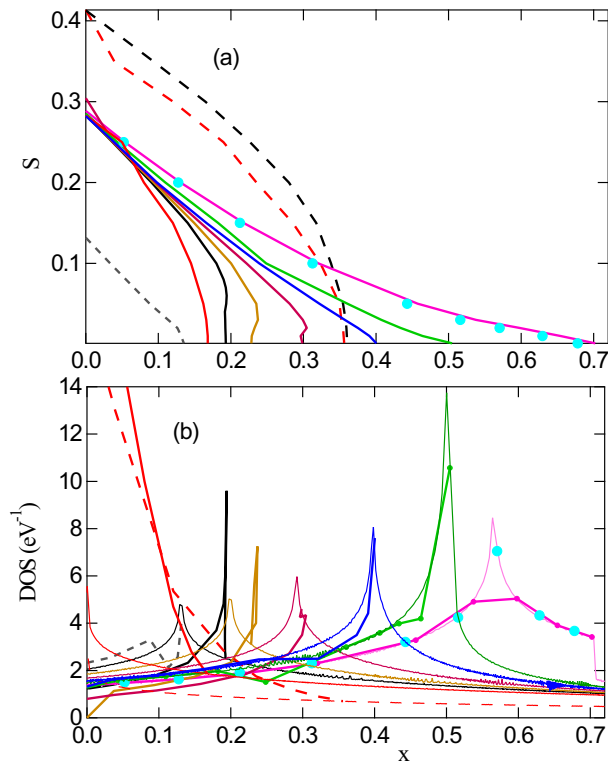


FIG. 1: (π, π) -AFM phase in cuprates. (a) AFM magnetization S and (b) corresponding DOS as a function of t' for several values of Hubbard U and renormalization Z : $U = 2\text{eV}$, $Z = 1$ (long-dashed lines), $U = 1\text{eV}$, $Z=0.5$ (solid lines), or $U = 0.5\text{eV}$, $Z=0.5$ (short-dashed line), with $t'/t = 0$ (red), -0.08 (black), -0.12 (brown), -0.17 (dark red), -0.22 (dark blue), -0.26 (light green), -0.32 (light blue dots), and -0.33 (magenta). In frame (b) the thin lines of the same color represent the corresponding nonmagnetic phases.

II. AFM DOS PEAK

We model the cuprates by a three-parameter tight-binding model, with the nearest t , the second-nearest t' , and the third-nearest neighbor t'' hopping parameters, of the form introduced by Pavarini and Andersen (PA), $t'' = -0.5t'$.⁷ While we mainly study properties as a function of t' , we note the following correspondences to the known monolayer cuprate families⁸: $t'/t \sim -0.12$ for $\text{La}_{2-x}\text{Sr}_x\text{CuO}_4$ (LSCO), -0.22 for $\text{Tl}-2\text{Ba}_2\text{CuO}_{6+\delta}$ (TBCO) and $\text{HgBa}_2\text{CuO}_{4+\delta}$ (HBCO), and -0.26 for $\text{Bi}_2\text{Sr}_2\text{CuO}_{6+\delta}$ (BSCO).

By incorporating spin fluctuation renormalization of the coherent electrons by a factor $Z \sim 0.5$ and the Coulomb screening of the Hubbard U to $\sim 1\text{eV}$,⁹ we can use a self-consistent Hartree-Fock calculation to determine the AFM phase diagrams, and the subtle role of the VHS in the lower magnetic band, Fig. 1. Details, including alternative choices of U and Z (dashed lines in Fig. 1), are in SM-A. In Fig. 1(a), we see that the dimensionless magnetization $S = \langle n_\uparrow - n_\downarrow \rangle / 2$ gives an average magnetic moment $\mu = 2S\mu_B = 0.6\mu_B$, where μ_B is the Bohr magneton, in good agreement with experiment^{10,11}. Since the intertwined orders in the pseudogap are associated with charged antiphase domain walls, which are weakened near the termination of AFM order, we can defer their discussion to Section IV and focus on the pure AFM phase.

Our key results are that (1) the AFM gap collapses close to the point where the AFM VHS crosses the fermi level. (2) Especially for small t' , this VHS (thick solid lines Fig. 1(b)) has a much stronger divergence than the NM VHS (thin solid lines). (3) In this regime the AFM gap collapse is first-order, as seen by the nonmonotonic $S(x)$ curve, and falls at a doping beyond the NM x_{VHS} . (4) For $t' \leq -0.2$ the NM VHS grows larger as it approaches a power-law divergence near $t' \sim -0.26$. At the same time the AFM transition becomes continuous and the AFM and NM VHSs converge. Indeed, for $t' \sim -0.33$ the transition is virtually invisible in the DOS, as discussed in SM-A.

These results, particularly 1-3, are in good agreement with heat capacity measurements of pseudogap collapse. In

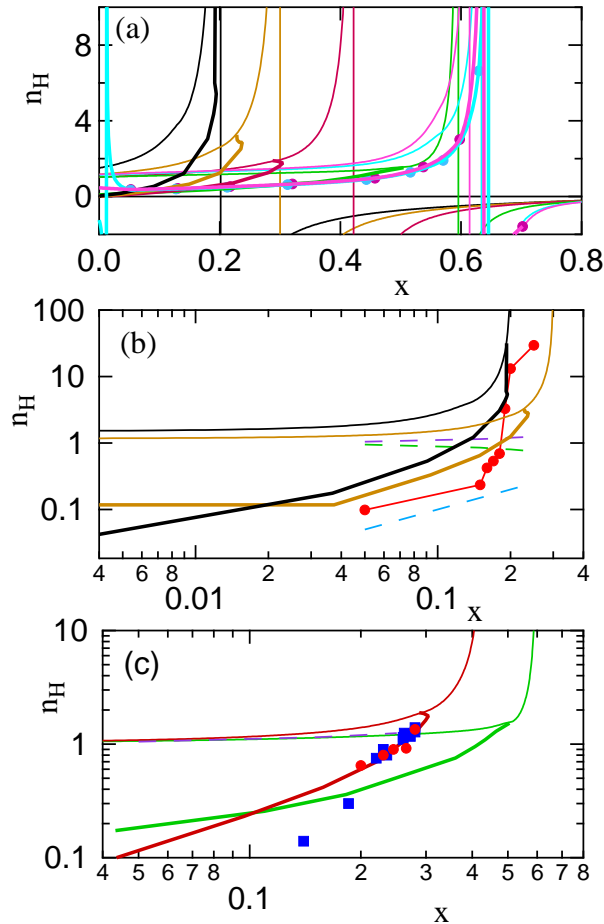


FIG. 2: Low-field Hall effect compared to experiment, showing (a) n_H , for the same parameter sets as in Fig. 1. (b) Comparison of the data for $t' = -0.08t$ (black curves) and $t' = -0.12t$ (brown curves) to experimental data on LSCO¹⁴ (red dots). Dashed lines illustrate n_H scaling as x (light blue), $1-x$ (green), or $1+x$ (violet). (c) Comparison of the theory for $t'/t = -0.26$ (green) and -0.17 (dark red curves) to experimental data on Bi- (red circles) and Tl-curates (blue squares)¹⁵.

particular, the simultaneous presence of strong DOS divergence and first order transition would seem to be incompatible – see the retrograde DOS curves in Fig. 1(b). Possible explanations for this are discussed in SM-A.1. A possible role of interlayer coupling is discussed in SM-A.2.

In the above discussion, we showed that AFM order persists to the largest $|t'/t|$ studied. However, for such large $|t'|$, there can be a competition between inter- and intra-VHS scattering, with the latter leading to a more conventional form of CDW. The latter is predicted to dominate for $t'/t \leq -0.23$,⁸ but so far there is little evidence for it.

III. LOW-FIELD HALL EFFECT

If the AFM pseudogap has a sharp quasi-discontinuous transition at doping x to a NM state, one expects a jump in fermi surface area from small, $\sim x$, to large $\sim 1-x$, which could show up in the Hall density. However, for low-field measurements the cyclotron frequency ω_c satisfies $\omega_c\tau \ll 1$, so the Hall coefficient $R_H = 1/n_H e$ is not sensitive to the fermi surface area, but to the average curvature. At a certain doping beyond x_{VHS} , $R_H \rightarrow 0$ and the Hall density diverges, Fig. 2(a). The transport results are worked out in SM-B; to focus on band structure effects, a doping- and t' -independent scattering rate is assumed, $\hbar/\tau = 1$ meV. In a one-band model, R_H and n_H should be relatively insensitive to the nature of the scattering, and the good agreement with experiment for LSCO¹⁴, Fig. 2(b), and the

monolayer Tl (blue squares) and Bi (red circles) cuprates¹⁵, Fig. 2(c), confirms this.

Figures 2(b,c) constitute another key result, demonstrating nearly quantitative agreement with experiment (although the value of t' is somewhat smaller than expected for the Bi- and Tl-cuprates). We briefly discuss the Tl-cuprate results, while additional comments are in SM-B. In the phenomenological model, doping in the pseudogap phase scales with x , then jumps rapidly to $1+x$ in the normal phase. Instead, we find that the doping dependence of n_H arises mainly from the gradual closing of the AFM gap. Notably, while the Tl-cuprates are generally assumed to represent the overdoped NM phase, we find that all data remain in the pseudogap phase. Consistent with our interpretation, it was recently found that monolayer Tl-cuprates host a CDW up to a doping $x_{CDW}=0.265$ ¹⁶, close to our $x_{pg}=0.29$. This CDW could be associated with the charged domain walls in the AFM phase. As to the large Fermi surface observed in QO measurements, it could be associated with magnetic breakdown of small gaps, while ARPES has a tendency to find large Fermi surfaces even in undoped cuprates, Section V.A.

Thus, the present model of the pseudogap as a form of short-range AFM order, which explains the anomalous VHS peak seen at the pseudogap collapse, also captures the anomalous growth of n_H with doping (albeit with some uncertainty about the optimal t' for each cuprate), two key features of pseudogap collapse. It also predicts the nearly step-like termination of the pseudogap. In the following Section, we will show how the associated strongly fluctuating topological defects can account for the observed intertwined order.

IV. COMPETING ORDERS IN THE CUPRATES

A. Overview of competing orders

Figure 3 compares the phase diagram of YBCO with related STM results on Bi2201, displaying the role of competing phases. Detailed discussion is in SM-C, leading to the following conclusions.

While charge order in cuprates seems to take the form of stripes at low doping and CDWs at high doping, a clear transition is not often found. First principles calculations⁵ shed light on this, finding uncharged antiphase domain walls in YBCO6 that evolve into charged domain walls in YBCO7. The uncharged walls are stripe-like, being purely repulsive and staying as far apart as possible, whereas the charged walls are CDW-like, having a minimum energy for a finite charge periodicity $P_c = 4$ (corresponding to 4 Cu atoms) which is approximately consistent with Fermi surface nesting. However, these CDWs are highly unconventional, since the dominant contribution to minimizing their energy involves maximizing the average magnetic moment. Thus, we propose that the stripe-CDW crossover consists of rearranging AFM domain walls, from staying as far apart as possible to adjusting their average spacing to match the (doping-dependent) Fermi surface nesting periodicity.

The natural locus for this charge-order transition is a commensurate-incommensurate transition in the electronic susceptibility, also called the Mott-Slater (M-S) transition since Fermi surface nesting is only found on the incommensurate side.¹⁷ This should be the second most prominent feature in the AFM phase diagram, and determining its location would provide additional confirmation for the theory. STM studies¹⁸ provide a valuable clue. The vertical black line in Fig. 3 defines the doping x_{CI} , where the charge order crosses over from commensurate nesting at $P_c=4$ Cu to incommensurate Fermi-surface nesting.

STM studies bring the roles of impurity clustering and nanoscale phase separation (NPS) into sharp focus. They typically find that sample surfaces consist of arrays of gap maps – roughly 3 nm patches with distinctly different combined pg-superconducting gaps covering the surface¹⁹. These gaps are found to correlate with distinctly different local doping, associated with clusters of a particular interstitial oxygen impurity²⁰. The roles of impurities and NPS will be discussed further below and in SM-D, and for now we simply assume that the most common gap size correlates with the dominant domain wall order at that average doping (blue symbols in Fig. 3 – see SM-C for details).

Thus, we find that (1) the dominant charge order phase consists of commensurate stripes with $P_c = 4$ periodicity, seen directly in the STM (blue squares at T_C) and as the onset of an electron Fermi surface pocket in the Hall effect (T_{max}), and correlated with the small pocket seen in quantum oscillation studies²¹. However, the persistence of a single Fermi surface over a doping range $0.08 < x < 0.18$ ²² is highly unusual, and suggests that the $P_c = 4$ stripes are present in the form of local patches which can percolate over an extended doping range, consistent with the STM results. (2) Ising AFM order in cuprates arises from small anisotropy of the Heisenberg exchange, which allows a finite temperature Neel transition. At a lower T there is an Ising to $X - Y$ transition, at which domain walls become unstable, leading to loss of stripe/CDW order. This can be identified with the curve T_H . (3) Since the AFM order can be long-range only in the Ising phase, the system transforms from short-range AFM order to potentially long-range CDW order (depending on the effect of disorder on the charged stripes) as T is reduced. (4) As a function of doping, there are several discontinuous transitions within the pseudogap phase, one at $x = 0.08$, and several between 0.14 – 0.19. These are discussed further in the following subsection.

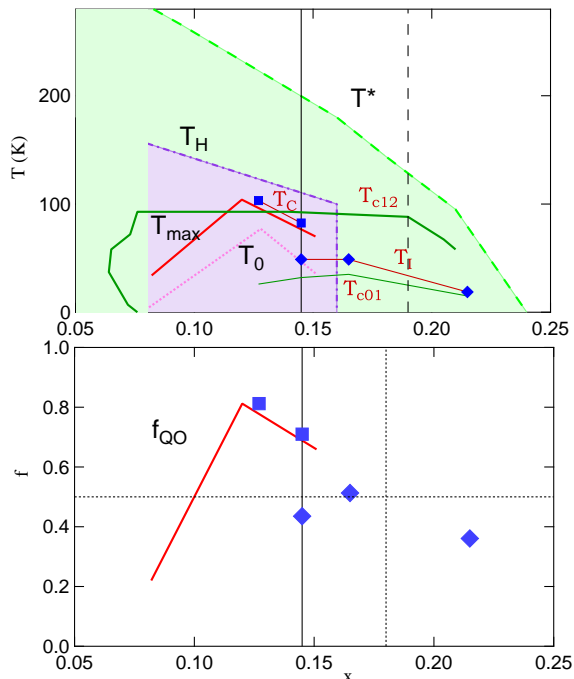


FIG. 3: **Domain wall evolution.** (a) Pseudogap phase diagram of YBCO, compared to STM results on Bi2201. For YBCO, T^* is the pseudogap onset, which we interpret as short-range (π, π) AFM order, while we interpret T_H as the Ising-X-Y transition, where domain walls become unstable, while T_{max} and T_0 refer to the appearance of patches of charge period 4 1D (or 2D) stripes. For Bi2201 T_s is the superconducting transition temperature, while the blue squares (T_C) and diamonds (T_I) track the peaks in the patch maps of commensurate and incommensurate stripe phases in different samples. The green curves labelled $T_{c(n-1)n}$ are the superconducting T_{cs} of Bi22(n-1)n, $n = 1, 2$. (b) Two estimates of the fraction of period 4 stripes, for YBCO (red line) and Bi2201 (blue squares), while blue diamonds estimate fraction of a competing phase.

B. Mott-Slater transition in the charge order

We interpret the small fermi surface found in quantum oscillations (QOs) and the curves T_{max} and T_C as evidence for a nanoscale $P_c = 4$ charge order phase, with the termination of the QOs near $x = 0.08$ and $x = 0.18$ ²² as percolative transitions. The regime below $x = 0.125$ was discussed earlier, in terms of the stripe evolution at low doping²³ replaced by nanoscale phase separation (NPS) involving the $P_c = 4$ stripes – see Fig. 14 of Ref. 24. Note that it involves the loss of superconductivity at lowest doping. Figure 3(b) sketches a simple picture of this phase nps, assuming that the $P_c = 4$ phase exists as a homogeneous phase only at $x = 0.125$, and away from that point T_C scales as the fraction f_{QO} present in the sample.

The region between $x = 0.14$ and 0.19 is much more complex, with possibly more than one transition and some material dependence. To unravel this, we focus on the components of the $P_c = 4$ phase. First, T_{max} in YBCO and T_C in Bi2201 both terminate abruptly near $x = 0.15$, but whereas nothing is found at higher doping in YBCO, there is an incommensurate branch T_I in Bi2201. In contrast, the QOs in YBCO extrapolate to an effective mass divergence at $x = 0.18$. One can formulate a consistent picture as follows: the $P_c = 4$ phase is heading toward a percolation crossover at $x = 0.18$ (intersection of crossed dashed lines in Fig. 3(b)), when this is interrupted by the Mott-Slater transition, which forms an incommensurate phase lacking the electron pocket. Note that the last doping at which the QOs are observed is $x = 0.15$, consistent with this picture.

For present purposes, the key result is that the Mott-Slater transition occurs near $x \sim 0.14 - 0.15$, and can be interpreted as a reorganization of the domain walls to capture fermi surface nesting. Thus, the q -vector for charge order in the incommensurate regime is consistent with fermi surface nesting, but inconsistent with the stripe ordering vectors in the low doping regime. To match the fermi surface q -vector requires fractional charge periodicity, for example $P_c \sim 4.6$, which can be achieved by the wall periodicity fluctuating between 4 and 5. Indeed, a recent STM study finds that the main defect in the nematic phase is the merging of two stripes into a single one, consistent with

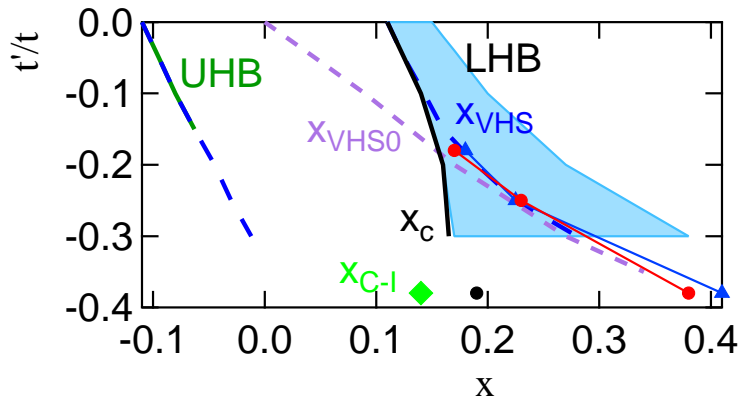


FIG. 4: Comparing calculated dopings of ‘pseudogap’ x_c (solid lines) and VHS x_{VHS} (dashed lines), vs t'/t (assuming $t'' = 0$)²⁷. Blue long-dashed lines indicate x_{VHS} , while x_{VHS0} (violet short-dashed line) is the bare VHS, which at low dopings drives the splitting of the bands into UHB and LHB; light-green diamond is x_{C-I} ; red dots and blue triangles represent experimental x_{pg} and x_{VHS} ²⁶.

the domain-wall model.²⁵

C. Mott-Slater transition vs VHS

While we have identified the Mott-Slater transition in the stripe ordering, it should play a significant role in the electronic states, potentially leading to an emergent spin liquid phase and a large drop in correlation length across the transition,¹⁷ which could be mistaken for a pseudogap collapse. Thus, when experiments²⁶ found that the pseudogap seems to terminate close to the doping x where the Van Hove singularity (VHS) crosses the Fermi level, $x_{pg} \sim x_{VHS}$, several theoretical calculations^{27,28} were able to reproduce this result only for $t' > t'_{cr}$, while for $t' < t'_{cr}$, $x_c < x_{VHS}$, Fig. 4. (To avoid confusion, we use the symbol x_c to denote the crossover doping that was identified as the pseudogap closing in Refs. 27,28.)

To compare these results with experiment²⁶, we plot Fig. 2 of Ref. 27 in Fig. 4, making use of a symmetry of the Hubbard model (under $x \rightarrow -x$ and $t' \rightarrow -t'$) to replot the data for $t' > 0$, $x > 0$ (hole doped, non-cuprate like) as $t' < 0$, $x < 0$ (electron doped cuprate-like). We first focus on the comparison between x_c (solid black and green lines) and the dressed x_{VHS} (long-dashed blue lines). These are in good agreement for electron-doping ($x < 0$) into the upper Hubbard band (UHB), but for hole-doping into the lower Hubbard band (LHB) the agreement lasts only for $t' > t'_c \sim -0.15$, while for smaller t' , $x_c < x_{VHS}$. However, x_c is in poor agreement with the experimental²⁶ x_{pg} (red circles), which are much closer to $x_{pg} = x_{VHS}$, as in Fig. 1(b). (We discuss in SM-C.4 how the experimental data are plotted here.) On the other hand, x_c is in reasonable agreement with x_{C-I} for Bi2201 (green diamond and black solid vertical line in Fig. 3(a)). The recent ARPES results for Bi2212 (black dot and black dashed vertical line in Fig. 3(a) and black dot in Fig. 4)²⁹ are also in better agreement with x_{C-I} than with the Hall effect estimates of x_{pg} . This experiment seems to be finding a loss of interlayer coherence, specifically loss of the splitting of the bilayer bands into a bonding-antibonding pair at low T .

The region between x_{C-I} and x_{VHS} is likely to be highly disordered, both because of frustration due to competing phases in the incommensurate regime, because the region of the $C - I$ -transition is expected to house a spin liquid phase, and because of strong scattering associated with the VHS. Hence the results of Ref. 30 offer some confirmation of the current assignments. There it is found that the light-blue shaded region in Fig. 4 is a strange metal Fermi liquid phase, with linear-in- T resistivity. Further evidence for x_{C-I} is presented in SM-C.4.

Note that x_{C-I} is close to the temperature of optimal superconductivity, suggesting that AFM-CDW competition, or the emergent spin glass phase is beneficial for superconductivity. See further SM-C.5.

V. DISCUSSION

A. Three VHSs?

Since the DOS of a saddle point VHS diverges when a 2D band crosses over from, e.g., hole-like to electron-like, the analog in the Hall effect would be the diverging n_H when the average local curvature crosses over from hole-like to electron-like. Thus, the present calculations predict three VHS crossings as doping is increased: first the NM VHS, then the AFM VHS, then the diverging n_H , with the latter two experimentally accessible via heat capacity and Hall effect respectively. Surprisingly, the NM VHS may be accessible via ARPES. For reasons that are not clear, ARPES seems to see the bare fermi surface even in undoped samples.³¹ Possible reasons are discussed in SM-E.1.

Note that this ARPES ghost fermi surface complicates the discussion of pseudogap collapse in the Tl-cuprates. While it is usually assumed that the large fermi surface seen in ARPES represents the true, NM fermi surface, our analysis of the Hall data, Fig. 2(c), indicates that all samples are still in the AFM phase, albeit with small gaps.

B. Remaining puzzles

1. Scattering rate

Given the above results, it is no wonder that the transport is anomalous. A texture of charged stripes can lead to an inhomogeneous and highly anisotropic resistivity. Added to that, oxygen impurity clustering leads to charge patches and further doping inhomogeneity (the gap maps). Thus, any measured τ is likely to suffer from inhomogeneous broadening, which may be different for different probes. Consistent with this, Dessau has demonstrated that the ARPES broadening is mainly inhomogeneous and the intrinsic broadening is much smaller³².

The proximity of a VHS to x_{pg} naturally reminds one of the early predictions that the VHS is responsible for the observed linear-in- T ³³ and $-\omega$ ³⁴ resistivity. Indeed, many of the predictions of VHS theory are quite similar to the predictions of marginal Fermi liquid theory³⁵, except that the latter assumes that τ is k -independent, while VHS scattering is expected to peak at (π, π) . Thus, early model calculations found T-linear scattering near (π, π) , but with quadratic deviations from other parts of the Fermi surface.³⁶ Many recent experimental studies find that resistivity in cuprates is hardly ever strictly linear, tending to be a mix of linear and quadratic^{37,38}. Indeed, Hussey finds that the scattering tends to be stronger and more linear near (π, π) , and more quadratic on the rest of the Fermi surface, thus favoring the VHS interpretation. Recent work supports the idea that the VHS is responsible for strange metal behavior in the related compound $\text{Sr}_3\text{Ru}_2\text{O}_7$.³⁹ A recent calculation on cuprates³⁰ finds linear-in- T resistivity over a strange metal phase which extends over a range of doping and t' values, blue shaded region in Fig. 4. Note that this region is approximately centered over $x_{VHS}(t')$.

2. Thermal Hall effect

A thermal Hall effect has been found in the pseudogap state of several cuprates⁴⁰. Since it is found in insulators, it is believed to be dominated by phonons [not magnons], and these would have to be chiral phonons.³ Recent evidence suggests that the ground state in most cuprates has lower symmetry than previously expected,^{41,42} and that this might be responsible for both chiral phonons and the anomalous Kerr effect, which also seems related to the pseudogap.⁴³

Intriguingly, in LSCO this lower symmetry is related to LTT-type structural distortions⁴⁴. This LTT order has uncompensated moments along the c -axis in each layer, which could account for the chirality. If the order is long-range, the moments cancel in alternate layers. However, at high temperatures the LTT order is only short-range, leading to short-range ferromagnetic order.

The LTT phase initially came into prominence because it splits the VHS degeneracy⁴⁵⁻⁴⁷. While this splitting is surprisingly small,⁴⁸ that is not uncommon for dynamical Jahn-Teller effects, which could be present in cuprates.⁴⁹

Thus, it seems likely that the phase responsible for chiral phonons is related to a short-range order stabilized by the VHS, at least in LSCO, whereas the nature of this phase remains unknown in other cuprates.

C. Comparison with earlier work

Some of the ideas of our model were anticipated in a short-range order model, where the holes are dressed by AFM fluctuations which produce a strongly enhanced VHS⁵⁰. The role of long- vs short-range order is not discussed in the

present paper, which is a zero-temperature, disorder-free calculation. Extending the calculation to finite temperatures requires accurately describing Mermin-Wagner physics^{17,51}, while treating disorder will require an understanding of nanoscale phase separation (NPS) (SM-D).

Our work bears some resemblance to the work of Yang *et al.*^{52,53}. They found that superconductivity is significantly enhanced near the cuprate quantum critical point (QCP) due to an enhanced (power-law) divergence in the particle-particle susceptibility⁵². They found that this could be explained by a VHS at the QCP, but only if the VHS is a high-order VHS with power-law $p \sim 0.5$.⁵³ However, the VHSs in NM cuprates are material dependent, varying from logarithmic to power law, but with $p \sim 0.25$ (analytically, near the VHS⁵⁴) or 0.29 (numerically, over a broad energy range⁸). In contrast, Michon *et al.*⁵⁵ find a heat capacity consistent with an enhanced but logarithmic VHS. Our work can reconcile these two results: we find that the AFM VHSs are close to a hoVHS with power law $p \sim 0.5$ ⁸, but at a slightly different doping. This means that at energies far from the VHS they grow with a power law ~ 0.5 , but as they approach the VHS they break off to a slower, logarithmic growth.

A glance at Fig. 1 illustrates what Michon *et al.* should have seen: the discontinuous drop of T^* at the end of the pseudogap x_{pg} , Fig. 3, should lead to a cut-off of the VHS peak. Instead, Michon *et al.* find a full VHS, albeit broadened over a quite wide doping range. This is discussed in detail in SM-A.1, where it is concluded that this may be another signature of NPS.

D. hoVHSs

In Ref.⁸, it was noted that the secondary hoVHS associated with AFM order arises from a highly unusual flat band fermi surface, a diamond running along the AFM zone boundary. It was speculated that such a flat band seemed to discourage rather than encourage instability, by forming a continuum of equally competing instability q -vectors. In the present paper we confirm that conjecture, showing that due to the AFM VHS, the AFM phase can extend well beyond the doping of the NM VHS. In practice, it does this by introducing arrays of topological defects – domain walls – which can mimic the effects of incommensurate SDWs and CDWs, and can change from one incommensurate q -vector to another by rearranging the domain walls without need of a conventional Landau phase transition.

VI. CONCLUSIONS

Earlier studies identified the pseudogap as a form of short-range AFM order⁹, with the lack of long-range order due to frustrations from lower dimensional fluctuations and competing instabilities¹⁷. In parallel, DFT studies found the important role of domain walls in generating anomalous stripe and CDW phases⁵. Here we have shown that the same models can explain key features of the pseudogap collapse, .

In this work, we focused on describing the underlying band structure effects, neglecting as far as possible the effects of heterogeneity, disorder, and scattering. This provides a framework upon which these factors can be subsequently incorporated. This is particularly important for the scattering, both because the effects of heterogeneity and dopant disorder will make it hard to extract the intrinsic scattering and because the electron-electron scattering is likely to be strongest near the VHS, making self-consistent calculations particularly difficult.

Given these simplifications, our model still captures many key features of the pseudogap collapse. We model the pseudogap collapse as a collapse of the underlying AFM order. We find striking agreement with several of the key signatures of pseudogap collapse, including the logarithmically diverging heat capacity associated with an AFM VHS, beyond which n_H remains positive and increases with x , although it is not directly the signature of a large fermi surface. Proximity of x_{pg} to a strong VHS suggests that the linear-in- T resistivity is associated with strong scattering at the VHS. Moreover, the often observed discontinuous drop of T^* to zero at x_{pg} also follows naturally from our model.

The big surprise in this calculation was in the Mott-Slater, or C-I transition. Working from the NM susceptibility one expects a crossover from AFM (dominated by q near (π, π) fluctuations) to CDW (q near Γ) fluctuations. However, the strong role of the AFM VHS reduces this to a crossover in the nature of domain wall ordering. Key evidence for this comes from DFT calculations⁵ plus the STM finding that the defect structure looks more like domain-walls than conventional CDWs.²⁵ It may be that in other systems – Fe-based superconductors or even in the cuprates with

largest $|t'|$ – charge order plays a larger role.

-
- ¹ Eduardo Fradkin, Steven A. Kivelson, and John M. Tranquada, “Theory of intertwined orders in high temperature superconductors”, *Rev. Mod. Phys.* **87**, 457 (2015).
 - ² Rafael M. Fernandes, Peter P. Orth, and Jörg Schmalian, Intertwined vestigial order in quantum materials: nematicity and beyond, *Annual Review of Condensed Matter Physics* **10**, 133 (2019).
 - ³ M. Lizaire, A. Legros, A. Gourgout, S. Benhabib, S. Badoux, F. Laliberté, M. -E. Boulanger, A. Ataei, G. Grissonnanche, D. LeBoeuf, S. Licciardello, S. Wiedmann, S. Ono, S. Kawasaki, G. -Q. Zheng, N. Doiron-Leyraud, C. Proust, and L. Taillefer, Transport signatures of the pseudogap critical point in the cuprate superconductor $\text{Bi}_2\text{Sr}_{2-x}\text{La}_x\text{CuO}_{6+\delta}$, *Phys. Rev. B* **104**, 014515 (2021).
 - ⁴ W. D. Wise, Kamallesh Chatterjee, M. C. Boyer, Takeshi Kondo, T. Takeuchi, H. Ikuta, Zhijun Xu, Jinsheng Wen, G. D. Gu, Yayu Wang and E. W. Hudson, Imaging nanoscale Fermi-surface variations in an inhomogeneous superconductor, *Nature Physics* **5**, 213 (2009).
 - ⁵ Yubo Zhang, Christopher Lane, James W. Furness, Bernardo Barbiellini, John P. Perdew, Robert S. Markiewicz, Arun Bansil, and Jianwei Sun, “Landscape of competing stripe and magnetic phases in cuprates”, *PNAS* **117**, 68 (2019).
 - ⁶ R.S. Markiewicz, Dispersion of ordered stripe phases in the cuprates, *Phys. Rev. B* **62**, 1252 (2000).
 - ⁷ E. Pavarini, I. Dasgupta, T. Saha-Dasgupta, O. Jepsen, and O.K. Andersen, Band-structure trend in hole-doped cuprates and correlation with T_{cmax} . *Phys. Rev. Lett.* **87**, 047003 (2001).
 - ⁸ Robert S. Markiewicz, Bahadur Singh, Christopher Lane, and Arun Bansil, High-order Van Hove singularities in cuprates and related high-Tc superconductors, arXiv:2105.04546.
 - ⁹ Das, T. Markiewicz, R.S. and Bansil, A., Intermediate coupling model of the cuprates, *Advances in Physics* **63**, 151-266 (2014).
 - ¹⁰ J. M. Tranquada, “Neutron scattering studies of antiferromagnetic correlations in cuprates,” in *Handbook of High Temperature Superconductivity*, pp. 257–298, Springer, Berlin, 2007.
 - ¹¹ Kanun Pokharel, Christopher Lane, James W. Furness, Ruiqi Zhang, Jinliang Ning, Bernardo Barbiellini, Robert S. Markiewicz, Yubo Zhang, Arun Bansil, Jianwei Sun, Sensitivity of the electronic and magnetic structures of cuprate superconductors to density functional approximations, arXiv:2004.08047.
 - ¹² Elbio Dagotto, Alexander Nazarenko, and Adriana Moreo, Flat quasiparticle dispersion in the 2D t - J model, *Phys. Rev. Lett.* **73**, 728 (1995).
 - ¹³ N. Bulut, D.J. Scalapino, and S.R. White, Quasiparticle dispersion in the cuprate superconductors and the two-dimensional Hubbard model *Phys. Rev. B* **50**, 7215 (1994).
 - ¹⁴ N. P. Ong, Z. Z. Wang, J. Clayhold, J. M. Tarascon, L. H. Greene, and W. R. McKinnon, Hall effect of $\text{La}_{2-x}\text{Sr}_x\text{CuO}_4$: Implications for the electronic structure in the normal state, *Phys. Rev. B* **35**, 8807(R) (1987).
 - ¹⁵ Carsten Putzke, Siham Benhabib, Wojciech Tabis, Jake Ayres, Zhaosheng Wang, Liam Malone, Salvatore Licciardello, Jianming Lu, Takeshi Kondo, Tsunehiro Takeuchi, Nigel E. Hussey, John R. Cooper, and Antony Carrington, Reduced Hall carrier density in the overdoped strange metal regime of cuprate superconductors, *Nat. Phys.* **17**, 826 (2021).
 - ¹⁶ C. C. Tam, M. Zhu, J. Ayres, K. Kummer, F. Yakhou-Harris, J. R. Cooper, A. Carrington, and S. M. Hayden, Charge density waves and Fermi-surface reconstruction in the clean overdoped cuprate superconductor $\text{Tl}_2\text{Ba}_2\text{CuO}_{6+x}$, *Nature Communications* **13**, 570 (2022).
 - ¹⁷ R.S. Markiewicz, I.G. Buda, P. Mistark, and A. Bansil, Entropic origin of pseudogap physics and a Mott-Slater transition in cuprates *Nature Scientific Reports* **7**, 44008 (2017).
 - ¹⁸ Tatiana A. Webb, Michael C. Boyer, Yi Yin, Debanjan Chowdhury, Yang He, Takeshi Kondo, T. Takeuchi, H. Ikuta, Eric W. Hudson, Jennifer E. Hoffman, Mohammad and H. Hamidian, Density wave probes cuprate quantum phase transition, *Phys. Rev. X* **9**, 021021 (2019).
 - ¹⁹ J. W. Alldredge, Jinho Lee, K. McElroy, M. Wang, K. Fujita, Y. Kohsaka, C. Taylor, H. Eisaki, S. Uchida, P. J. Hirschfeld, and J. C. Davis, Evolution of the electronic excitation spectrum with strongly diminishing hole-density in superconducting $\text{Bi}_2\text{Sr}_2\text{CaCu}_2\text{O}_{8+\delta}$, *Nature Physics*, **4** 319 (2008).
 - ²⁰ I. Zeljkovic, Z. Xu, J. Wen, G. Gu, R.S. Markiewicz, and J.E. Hoffman, *Science* **337**, 320 (212).
 - ²¹ N. Harrison and S.E. Sebastian, Protected Nodal Electron Pocket from Multiple-Q Ordering in Underdoped High Temperature Superconductors, *Physical Review Letters* **106**, 226402 (2011).
 - ²² B.J. Ramshaw, S.E. Sebastian, R.D. McDonald, J. Day, B.S. Tan, Z. Zhu, J.B. Betts, R. Liang, D.A. Bonn, W.N. Hardy, and N. Harrison, Quasiparticle mass enhancement approaching optimal doping in a high-Tc superconductor, *Science* **348**, 317 (2015).
 - ²³ M. Fujita, K. Yamada, H. Hiraka, P. M. Gehring, S. H. Lee, S. Wakimoto, and G. Shirane, Static magnetic correlations near the insulating-superconducting phase boundary in $\text{La}_{2-x}\text{Sr}_x\text{CuO}_4$, *Phys. Rev. B* **65**, 064505 (2002).
 - ²⁴ R. S. Markiewicz and C. Kusko, Phase separation models for cuprate stripe arrays, *Phys. Rev. B* **65**, 064520 (2002).
 - ²⁵ A. Mesáros, K. Fujita, H. Eisaki, S. Uchida, J. C. Davis, S. Sachdev, J. Zaanen, M. J. Lawler, and Eun-Ah Kim, Topological Defects Coupling Smectic Modulations to Intra-Unit-Cell Nematicity in Cuprates, *Science* **333**, 426 (2011).
 - ²⁶ N. Doiron-Leyraud, O. Cyr-Choinière, S. Badoux, A. Ataei, C. Collignon, A. Gourgout, S. Dufour-Beauséjour, F.F. Tafti, F. Laliberté, M.-E. Boulanger, M. Matusiak, D. Graf, M. Kim, J.-S. Zhou, N. Momono, T. Kurosawa, H. Takagi, Louis

- Taillefer Pseudogap phase of cuprate superconductors confined by Fermi surface topology Nature Communications 8, 2044 (2017)
- ²⁷ Wei Wu, Mathias S. Scheurer, Shubhayu Chatterjee, Subir Sachdev, Antoine Georges, and Michel Ferrero, Pseudogap and Fermi surface topology in the two-dimensional Hubbard model, Phys. Rev. X 8, 021048 (2018).
- ²⁸ Braganca, H. Sakai, S. Aguiar, M.C.O. and Civelli, M. Correlation-driven Lifshitz transition at the emergence of the pseudogap phase in the two-dimensional Hubbard model Phys. Rev. Lett. 120, 067002 (2018).
- ²⁹ Incoherent strange metal sharply bounded by a critical doping in Bi2212, Su-Di Chen, Makoto Hashimoto, Yu He, Dongjoon Song, Ke-Jun Xu, Jun-Feng He, Thomas P. Devereaux, Hiroshi Eisaki, Dong-Hui Lu, Jan Zaanen, and Zhi-Xun Shen, Science 366, 1099 (2019).
- ³⁰ Wei Wu, Xiang Wang, and André-Marie Tremblay, Non-Fermi liquid phase and linear-in-temperature scattering rate in overdoped two dimensional Hubbard model, PNAS 113, e2115819119 (2022) (arXiv:2109.02635).
- ³¹ S. Sahrakorpi, R. S. Markiewicz, Hsin Lin, M. Lindroos, X. J. Zhou, T. Yoshida, W. L. Yang, T. Kakeshita, H. Eisaki, S. Uchida, Seiki Komiya, Yoichi Ando, F. Zhou, Z. X. Zhao, T. Sasagawa, A. Fujimori, Z. Hussain, Z. -X. Shen, and A. Bansil, Appearance of Universal Metallic Dispersion in a Doped Mott Insulator, Phys. Rev. B 78, 104513 (2008).
- ³² T. J. Reber, N. C. Plumb, Y. Cao, Z. Sun, Q. Wang, K. P. McElroy, H. Iwasawa, M. Arita, J. S. Wen, Z. J. Xu, G. Gu, Y. Yoshida, H. Eisaki, Y. Aiura, D. S. Dessau, Pre-pairing and the "Filling" Gap in the Cuprates From the Tomographic Density of States, Phys. Rev. B 87, 060506(R) (2013).
- ³³ P.A. Lee and N. Read, Why is T_c of the oxide superconductors so low?, Phys. Rev. Lett. 58, 2691 (1987).
- ³⁴ R.S. Markiewicz, Comment on 'Carrier-carrier scattering in high- T_c superconductors', Phys. Rev. Lett. 62, 603 (1989).
- ³⁵ C.M. Varma, P.B. Littlewood, S. Schmitt-Rink, E. Abrahams and A.E. Ruckenstein, Phenomenology of the normal state of Cu-O high-temperature superconductors, Phys. Rev. Lett. 63, 1996 (1989).
- ³⁶ R. Hlubina and T. M. Rice, Resistivity as a function of temperature for models with hot spots on the Fermi surface, Phys. Rev. B 51, 9253 (1995).
- ³⁷ Keiichi Harada, Yuki Teramoto, Tomohiro Usui, Kenji Itaka, Takenori Fujii, Takashi Noji, Haruka Taniguchi, Michiaki Matsukawa, Hajime Ishikawa, Koichi Kindo, Daniel S. Dessau, and Takao Watanabe, Revised phase diagram of a high- T_c cuprate superconductor revealed by anisotropic transport measurements, arXiv:2109.11799.
- ³⁸ N. E. Hussey, J. Buhot, and S. Licciardello, A Tale of Two Metals: contrasting criticalities in the pnictides and hole-doped cuprates, Rev. Prog. Phys. 81, 052501 (2018).
- ³⁹ Connie H. Mousatov, Erez Berg, and Sean A. Hartnoll, Theory of the strange metal $\text{Sr}_3\text{Ru}_2\text{O}_7$, PNAS 117, 2852 (2020).
- ⁴⁰ G. Grissonnanche, S. Thériault, A. Gourgout, M. -E. Boulanger, E. Lefrançois, A. Ataei, F. Laliberté, M. Dion, J. -S. Zhou, S. Pyon, T. Takayama, H. Takagi, N. Doiron-Leyraud, and L. Taillefer, Phonons become chiral in the pseudogap phase of cuprates, Nature Physics 16, 1108 (2020).
- ⁴¹ A. de la Torre, K. L. Seyler, L. Zhao, S. Di Matteo, M. S. Scheurer, Y. Li, B. Yu, M. Greven, S. Sachdev, M. R. Norman, and D. Hsieh, Anomalous mirror symmetry breaking in a model insulating cuprate $\text{Sr}_2\text{CuO}_2\text{Cl}_2$, Nature Physics 17, 777 (2021).
- ⁴² A. de la Torre, S. Di Matteo, D. Hsieh, and M. R. Norman, Implications of second harmonic generation for hidden order in $\text{Sr}_2\text{CuO}_2\text{Cl}_2$, Phys. Rev. B 104, 035138 (2021).
- ⁴³ J. Xia, E. Schemm, G. Deutscher, S. A. Kivelson, D. A. Bonn, W. N. Hardy, R. Liang, W. Siemons, G. Koster, M.M. Fejer and A. Kapitulnik, Polar Kerr-Effect Measurements of the High-Temperature $\text{YBa}_2\text{Cu}_3\text{O}_{6+x}$ Superconductor: Evidence for Broken Symmetry near the Pseudogap Temperature, Phys. Rev. Lett. 100, 127002 (2008).
- ⁴⁴ A. Sapkota, T. C. Sterling, P. M. Lozano, Yangmu Li, HuiBo Cao, V. O. Garlea, D. Reznik, Qiang Li, I. A. Zaliznyak, G. D. Gu, and J. M. Tranquada, Reinvestigation of crystal symmetry and fluctuations in La_2CuO_4 , Phys. Rev. B 104, 014304 (2021).
- ⁴⁵ R.S. Markiewicz, Structural phase transitions and superconductivity in $\text{La}_{2-x}\text{A}_x\text{CuO}_4$, A=Sr,Ba J. Phys. Condens. Matt. 2, 6223 (1990).
- ⁴⁶ S. Barisic and J. Zelenko, Sol. St. Commun. 74, 367 (1990).
- ⁴⁷ W.E. Pickett, R.E. Cohen and H. Krakauer, Lattice instabilities, isotope effect, and high- T_c superconductivity in $\text{La}_{2-x}\text{Ba}_x\text{CuO}_4$, Phys. Rev. Lett. 67, 228 (1991).
- ⁴⁸ B. Büchner, M. Breuer, A. Freimuth and A.P. Kampf, Critical Buckling for the Disappearance of Superconductivity in Rare-Earth-Doped $\text{La}_{2-x}\text{Sr}_x\text{CuO}_4$, Phys. Rev. Lett. 73, 1841 (1994).
- ⁴⁹ R.S. Markiewicz, Van Hove excitons and high-T, superconductivity VIIIIC. Dynamic Jahn-Teller effects versus spin-orbit coupling in the LTO phase of $\text{La}_{2-x}\text{Sr}_x\text{CuO}_4$, Physica C 210, 235 (1993).
- ⁵⁰ Elbio Dagotto, Alexander Nazarenko, and Adriana Moreo, Antiferromagnetic and van Hove Scenarios for the Cuprates: Taking the Best of Both Worlds, Phys. Rev. Lett. 74, 310 (1995).
- ⁵¹ N.D. Mermin and H. Wagner, Absence of ferromagnetism or antiferromagnetism in one- or two-dimensional isotropic Heisenberg models, Phys. Rev. Lett., 17, 1133 (1966).
- ⁵² K.-S. Chen, S. Pathak, S.-X. Yang, S.-Q. Su, D. Galanakis, K. Mielson, M. Jarrell, and J. Moreno, Role of the van Hove Singularity in the Quantum Criticality of the Hubbard Model, Phys. Rev. B 84, 245107 (2011).
- ⁵³ S.-X. Yang, H. Fotso, S.-Q. Su, D. Galanakis, E. Khatami, J.-H. She, J. Moreno, J. Zaanen, and M. Jarrell, Proximity of the Superconducting Dome and the Quantum Critical Point in the Two-Dimensional Hubbard Model, PRL 106, 047004 (2011).
- ⁵⁴ R. Zehyer, Transition temperature and isotope effect near an extended van Hove singularity, Z. Phys. B97, 3 (1995).
- ⁵⁵ B. Michon, C. Girod, S. Badoux, J. Kamark, Q. Ma, M. Dragomir, H. A. Dabkowska, B. D. Gaulin, J. -S. Zhou, S. Pyon, T. Takayama, H. Takagi, S. Verret, N. Doiron-Leyraud, C. Marcenat, L. Taillefer, and T. Klein, Thermodynamic signatures

of quantum criticality in cuprates, Nature 567, 218 (2019).

Acknowledgements

This work is supported by the US Department of Energy, Office of Science, Basic Energy Sciences grant number DE-FG02-07ER46352, and benefited from Northeastern University's Advanced Scientific Computation Center (ASCC) and the allocation of supercomputer time at NERSC through grant number DE-AC02-05CH11231. We thank Adrian Feiguin for stimulating discussions.

Author contributions

R.S.M. and A.B. contributed to the research reported in this study and the writing of the manuscript.

Additional information

The authors declare no competing financial interests.

Theory of Cuprate Pseudogap as Antiferromagnetic Order with Domain Walls Supplementary Material

R.S. Markiewicz and A. Bansil¹

¹ Physics Department, Northeastern University, Boston MA 02115, USA

PACS numbers:

SM-A. AFM PHASE TRANSITION

We calculate the AFM doping dependence via a self-consistent (in density and magnetic moment) Hartree-Fock calculation, informed by many-body perturbation theory and *ab initio* calculations. Thus, analysis of the QPGW self-energy¹ finds that (1) while the Hubbard $U \sim 2\text{eV}$ for undoped cuprates, with doping it is screened by long-range Coulomb fluctuations, falling very rapidly or discontinuously to $\sim 1\text{ eV}$; (2) for finite doping the coherent dispersion is renormalized by a factor $Z \sim 0.5$, which also renormalizes U . (3) The renormalization turns on below an incoherent-to-coherent crossover energy/temperature scale associated with a peak in the imaginary self-energy. By confining our results to the low temperature coherent regime, we can work with fixed $U = 3t$, $Z = 0.5$ (solid lines in Fig. 1), with a generic bare $t=0.42\text{eV}$.

In Fig. 1(a), we define a dimensionless magnetization S by $\Delta = US$, $S = \langle n_{\uparrow} - n_{\downarrow} \rangle / 2$, and the average $\langle \dots \rangle$ is over occupied k -states. The efficacy of our self energy correction is clear: at low doping all curves converge to $S = 0.3$, giving an average magnetic moment $\mu = 2S\mu_B = 0.6\mu_B$, where μ_B is the Bohr magneton, in good agreement with experiment^{2,3}, while the gap parameter is $2\Delta = 0.76\text{eV}$, close to the experimental 1eV .^{4,5} In contrast, the bare $U = 6t$ and $Z = 1$ (long dashed lines) lead to too large values for S .

Moreover, first-principles calculations^{4,6} suggest that the intertwined order found in the pseudogap phase is as-

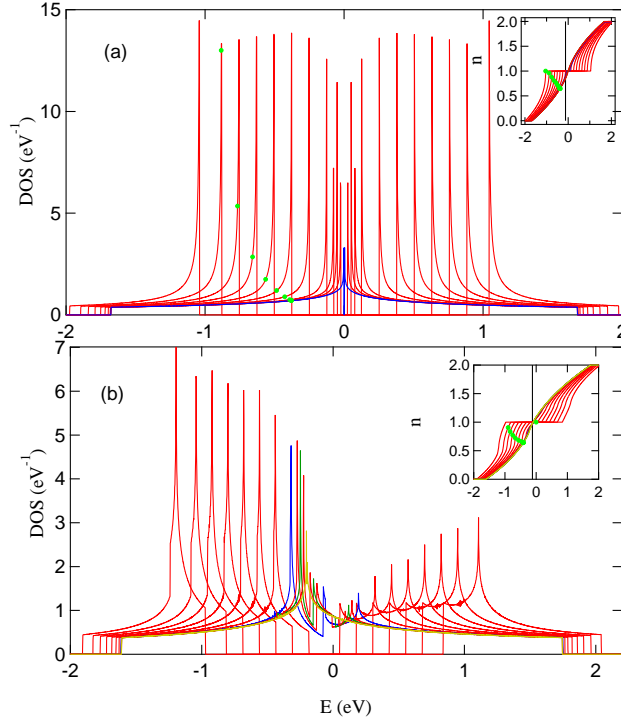


FIG. S1: Merging of VHSs of upper and lower magnetic bands at AFM collapse. Blue curves indicate initial gap closing. Insets show corresponding electron density n , with green dots indicating Fermi level.

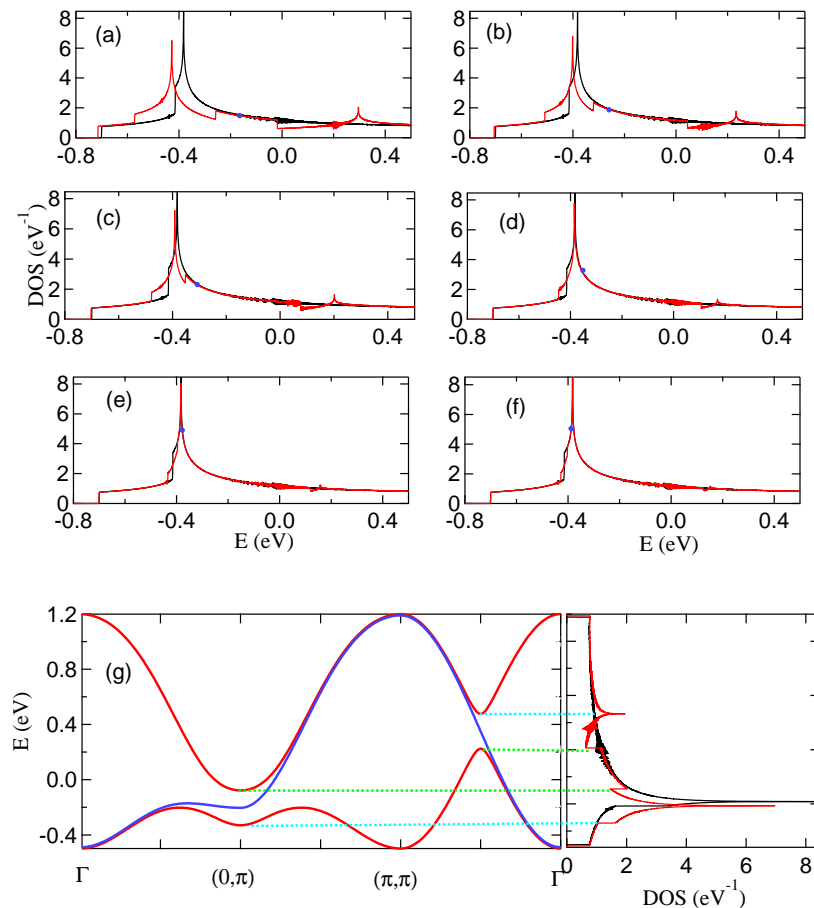


FIG. S2: **Hidden phase transition.** (a-f) DOS vs energy for increasing doping in AFM phase (red curves) vs nonmagnetic phase (black curves), with $S = 0.25$ (a), 0.15 (b), 0.1 (c), 0.05 (d), 0.03 (e), and 0.02 (f). Blue diamond indicates Fermi energy of AFM phase. (g) Dispersion vs DOS for data of frame (a).

sociated with topological defects of the AFM order, specifically antiphase domain walls, which become charged in doped cuprates. Domain walls are only topological defects in Ising antiferromagnets, associated in cuprates with small anisotropies of the exchange constant J . As the pseudogap weakens with temperature or doping, the Ising order is lost, and with it the domain-wall induced stripe or CDW order. Hence, these competing orders can be neglected in our calculations, where the principal emphasis is to understand the pseudogap collapse with doping. Effects of the domain walls are discussed in Section IV.

As the AFM gap collapses, a key role is played by the VHSs of the upper and lower magnetic bands (U/LMBs), Fig. S1, and how they evolve with doping. For the original Hubbard model with $t' = 0$, Fig. S1(a), the process is simple. The VHS of the LMB falls at the top of the band and the VHS of the UMB falls at band bottom. With doping the DOSs of the two bands approach one another virtually without change of shape, but with gradually reducing amplitude, until they merge into a single peak as the AFM magnetization $S \rightarrow 0$, Fig. S1(a). The need for a self-consistent calculation can be understood from this figure. The gap is stabilized because the electronic kinetic energy is lowered in the gapped phase, and most of that energy lowering is associated with electrons near the VHS of the LMB. Since the magnetic VHS is at the top of the LMB, hole-doping the sample moves the VHS above the fermi level, and the large electronic stabilization energy is quickly lost, causing the gap to collapse.

The case for finite t' is much more interesting, Fig. S1(b). With increasing doping, spectral weight in the UMB shifts from the saddle point VHS to the leading edge, causing it to peak at the bottom of the UHB, while the VHS of the LMB grows stronger as it moves toward the top of the band. At the same time, the two bands approach one another, until as $S \rightarrow 0$, the leading edge of the UMB merges with the saddle-point VHS of the LMB to form a single peak. In contrast, the saddle-point VHS of the UMB shrinks and merges with the leading edge of the LMB to form

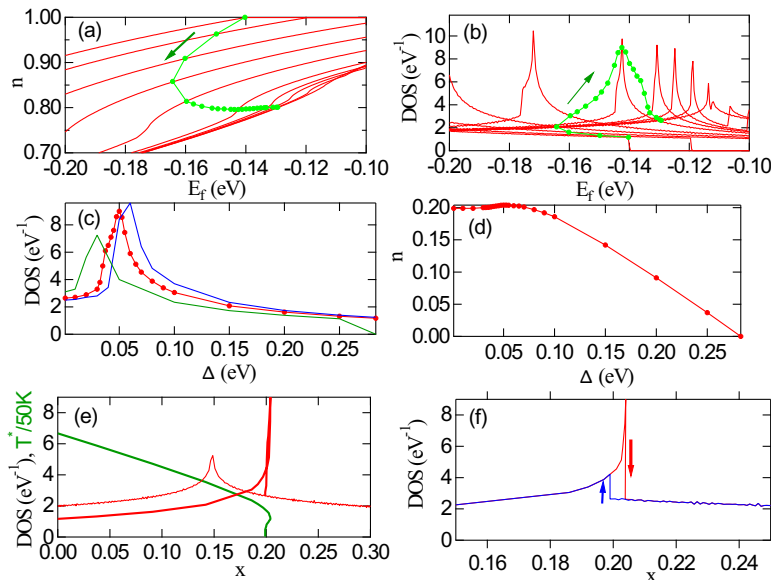


FIG. S3: **AFM DOS near x_{pg}** , for $t' = -0.09t$. (a,b) Band filling n (a) and DOS (b) evolution with gap parameter Δ , where green dots represent self-consistent E_f for different Δ , and the green arrows indicate the direction of decreasing Δ (equivalently, increasing hole doping). (c,d) Resulting DOS (c) and hole doping x (d) vs Δ . In (c), lower-resolution DOSs are shown for $t'/t = -0.08$ (blue) and -0.12 (green). (e) DOS (red) and T^* (calculated from Eq. S3 using $X = 24.8$ to approximate experiment) vs x . The nonmonotonic evolution of T^* and Δ indicates a first order transition. (f) Corrected DOS in case of maximum hysteresis, with arrows indicating sweep directions.

a featureless background. As seen in Fig. 1, the LMB VHS is in general distinct from the VHS of the nonmagnetic (NM) band, with the gap closing at a doping higher than x_{VHS}^{NM} .

The effect of this VHS collapse on the AFM order depends sensitively on the magnitude of U , Fig. 1. In Figure 1, the black curves (for $t' = -0.08t$) compare the doping evolution for several parameter values: unrenormalized $U = 6t$, $Z=1$ (long-dashed curve) vs $Z = 0.5$ and either $U = 3t$ (solid line) or $U = 1.5t$ (short-dashed line). For the first case, the NM VHS (thin black line in Fig. 1(b)) is far from the Fermi level when $S \rightarrow 0$, so the NM VHS has little effect on the transition. However, for the smaller U , the AFM VHS first approaches the NM VHS, when $U = 3t$, and crosses it near $U = 1.5t$. Note that whereas the NM VHS has a weak logarithmic divergence, the AFM VHS is close to a high-order VHS with strong power-law divergence. Note further that the gap collapse is first-order, as seen by the nonmonotonic $S(x)$ curve.

The remaining curves in Fig. 1 illustrate the strong evolution of the magnetic moment decay and the DOS with t' . We note that the first-order transition changes to second-order around $t' = -0.2t$. The $t' = -0.32$ and $-0.33t$ data are particularly interesting. There is a strong magnetic moment which decays to zero, but with *no sign of any transition in the DOS, which is identical to the nonmagnetic case*. This is a remarkable example of a hidden phase transition associated with a VHS, as illustrated in Fig. S2. The energy lowering arises from pushing the VHS peaks away from the Fermi level, but at low energies the two magnetic bands overlap (green dotted lines in Fig. S2(g)), creating a DOS that is virtually indistinguishable from the nonmagnetic DOS.

SM-A.1. AFM VHS line shape

In Fig. S3, we study the first-order AFM transition in more detail, using $t'/t = -0.09$ as an example. For each gap parameter Δ , the $T = 0$ dispersion is calculated and used to find the fermi energy at which the self-consistency equation for Δ is satisfied, from which the band filling n and the DOS are calculated, frames (a,b). Each green dot indicates a separate calculation at a different Δ . Note that as the AFM VHS approaches the Fermi level, it pushes the value of n backwards, like a wave pushing a floating log back towards the shore. In frames (c,d), we see that the DOS and doping $x = 1 - n$ are smooth functions of Δ . However, Δ and the resulting T^* , green line in frame (e), are not monotonic functions of x , and the regime where $\Delta(x)$ has three values indicates a first-order instability. Frame

(f) illustrates the maximum possible hysteresis one could have, showing that part of the DOS peak is cut off. Indeed, since hysteresis is not observed, the resulting first-order step should be calculated by a Maxwell construction, which would lead to a step roughly half way between the two hysteretic branches, in which case most of the DOS peak would be lost.

Thus, while the presence of an enhanced VHS at the AFM transition and the sharp step in T^* are both individually in good agreement with experiment, something goes wrong when we try to put them together: the step cuts off much of the DOS peak. Is there a way out of this problem? The strong swings in E_f , frames (a,b) are characteristic of an isolated system, lacking a particle reservoir. But in a system with NPS, such as the gap maps, the other patches can serve as a reservoir. Indeed, since each patch corresponds to a particular gap, each patch near x_{pg} will have a particular DOS, frame (c). The disorder will also smear out the backbending of the hole doping, frame (e). In this case, experiment should find a DOS peak similar to the peaks in frame (b), but broadened out by the distribution of oxygen environments. From the spread of the QO peak in Fig. 3 (the T_{max} line), this can amount to $\Delta x \sim 0.08$. This broadened DOS captures the features of the experimental heat capacity.

SM-A.2. c-axis dispersion

Recently, additional evidence was adduced that the observed heat capacity peak at pg collapse could not be associated with the normal state VHS in LSCO. ARPES finds a c-axis contribution to the electronic dispersion, of peculiar form associated with the body-centered tetragonal (BCT) form of Cu stacking in adjacent planes.⁷ This c-axis dispersion cuts off the divergence of the VHS peak altogether, leaving behind a flat topped peak.

Here we note that complications of c-axis dispersion should be much weaker in the AFM phase. First, in the pure AFM phase, the BCT stacking frustrates interlayer magnetic coupling, as a given Cu on one layer has equal numbers of nearest neighbor up and down spins on the next layer. Secondly, the stripe phase in LSCO has an unusual period quadrupling along the c-axis. This is generally interpreted in terms of coupling to (usually fluctuating) regions of low-temperature tetragonal order, which causes the stripe order to run alternately along the a- or b-axes in adjacent layers. The remaining period doubling is due to the parallel charge stripes on every other layer shifting laterally to remain as far apart as possible to minimize Coulomb repulsion. Both of these effects are readily seen to reduce interlayer hopping, particularly since the doped holes are mainly confined to the charged stripes.

Finally, we note that in the related compound $\text{La}_{2-x}\text{Ba}_x\text{CuO}_4$, the stripes have long-range order, which quenches superconductivity, particularly near $x = 0.125$. In the vicinity of the stripe order, strong *two-dimensional* superconducting fluctuations have recently been discovered.⁸

SM-B. LOW-FIELD TRANSPORT AND HALL EFFECT

We next analyze low-field transport, using the Kubo formulas

$$\sigma_{ij} = \frac{-2e^2}{c\hbar^2} \int \tau \frac{\partial f}{\partial E} \frac{\partial E}{\partial k_i} \frac{\partial E}{\partial k_j} \frac{d^2 k}{(2\pi)^2}, \quad (\text{S1})$$

$$\sigma_{ijk} = \frac{-2e^2}{c\hbar^2} \int \tau \frac{\partial f}{\partial E} \frac{\partial E}{\partial k_i} \epsilon_{krs} \frac{\partial E}{\partial k_r} \frac{\partial}{\partial k_s} \left(\tau \frac{\partial E}{\partial k_j} \right) \frac{d^2 k}{(2\pi)^2}, \quad (\text{S2})$$

where τ is the scattering time, σ_{ij} is the zero-field transport, and $\sigma_{ijk} H_k$ is the Hall conductivity with magnetic field $\vec{H} = H\hat{z}$. The same formula is used for the NM band and the two AFM bands, except that in the latter case each point is multiplied by a coherence factor, which adds up to one when summed over the two corresponding k -points of the U/LMBs. Fig. S4 shows our results, again with the thick lines in the AF phase and the thin lines in the NM phase. Since we are mainly interested in the effects of band structure on transport, we simplify the calculations by working at fixed $H = 1\text{T}$, $T = 100\text{K}$, and assume weak impurity scattering, $\hbar/\tau = 1\text{ meV}$ for all curves. Fig. S4(c) shows that for $H < 10\text{T}$ the cuprates are indeed in the low field limit. We note that for $t' > -0.26t$ there is a gap in the DOS at half filling, $x = 0$, so that the conductivity vanishes, Fig. S4(a), whereas for $t' = -0.26t$ the gap just closes and for smaller t' the UMB and LMB overlap, leading to finite σ_{xx} at $x = 0$. This is consistent with experiment, in that for the Bi cuprates, with $t'/t \sim -0.26$, a gap can be opened only when the Ca is replaced by a rare earth atom.⁹

The main result of this calculation is that for each t' there is a doping x_{H0} at which the Hall conductivity $\sigma_{xy} = 0$, Fig. S4(b). Consequently, the Hall angle $\omega_c \tau = \sigma_{xy}/\sigma_{xx}$, Fig. S4(c) and resistivity $\rho_{xy} = -\sigma_{xy}/(\sigma_{xx})^2 = R_H H$, Fig. S4(d), with $R_H = 1/(n_H e)$, also pass through zero at the same doping, so that $n_H \rightarrow \infty$, Fig. S5(b). Since

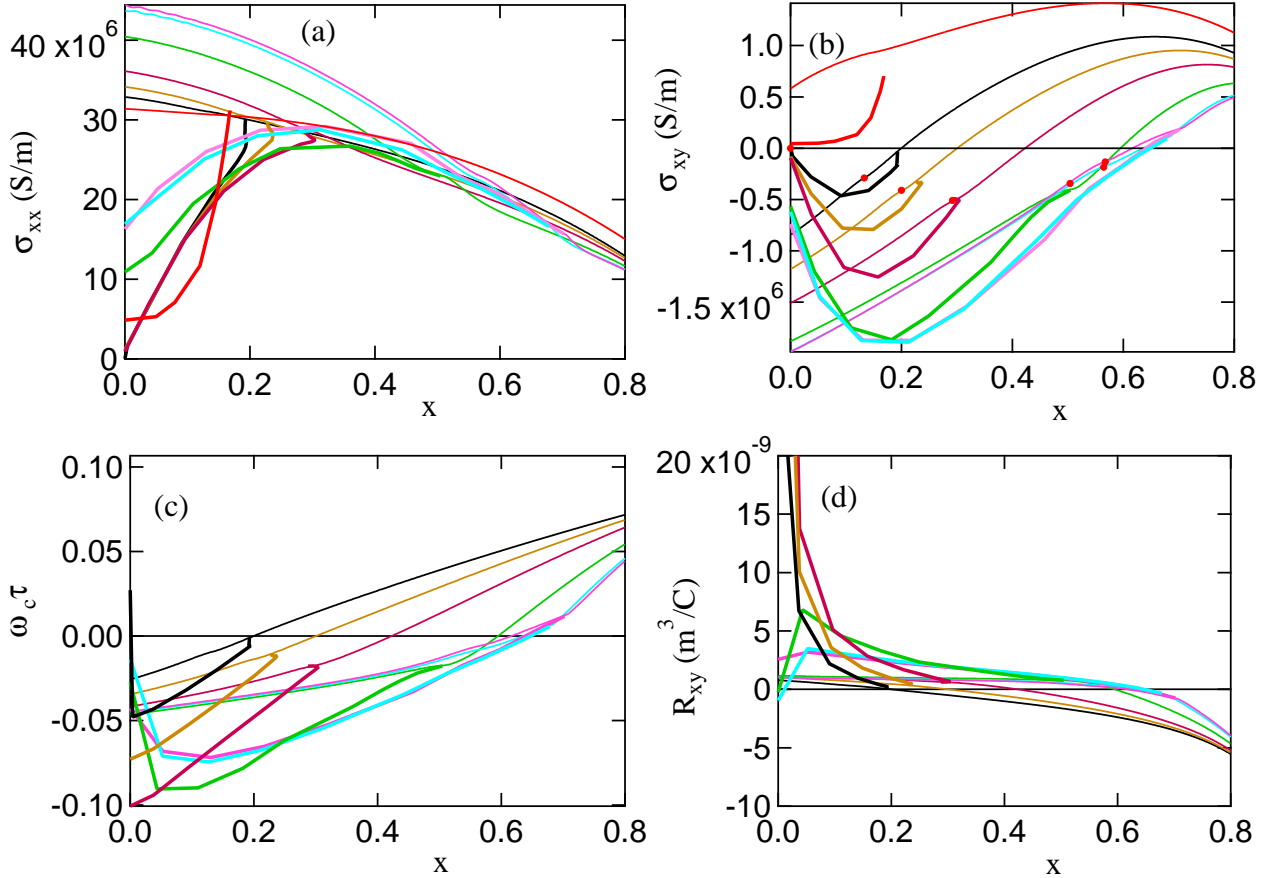


FIG. S4: Low-field Hall effect for the Pavarini-Andersen reference family of cuprates, for several values of t' , showing (a) σ_{xx} , (b) σ_{xy} , (c) $\omega_c\tau$, (d) ρ_{xy} , and (e) $|n_H|$. Color scheme of curves is consistent with Fig. ??.

this crossover involves a change from hole-like to electron-like conductivity, one might infer that it happens at the VHS, $x_{H0} = x_{VHS}$. One would be wrong. The low-field Hall conductivity is insensitive to the global nature of the Fermi surface – electron-like or hole-like – since $\omega_c\tau < 1$. Instead, the Hall conductivity is sensitive to the local curvature, and the Hall zero arises when the Fermi surface has equal amounts of positive and negative curvature. This is illustrated in Fig. S5(f), which displays the Fermi surfaces at each Hall zero. The red dots in Fig. S4(b) represent x_{VHS}^{NM} , showing that $x_{H0} = x_{VHS}^{NM}$ only in the Hubbard limit $t' = 0$.

Figures S5 and 2(b) show a key result, a comparison of our predicted resistivity and Hall density with the measured¹⁰ Hall resistivity in LSCO, compared to theory for $t'/t = -0.08$ or $t'/t = -0.12$. Figures S5(a,b) show the evolution with t' , while Figs. S5(c,d) and 2(b) are specific to LSCO. Our calculated resistivity is in good agreement with ρ_{xx} calculated for the commonly used model $\sigma_{xx} = ne^2\tau/m$ (black dashed line in frame (c)), with $m = 4m_0$, and m_0 is the free electron mass. By choosing a constant $\tau = \hbar/\gamma_0$, with $\gamma_0 = 1$ meV, we can extract the experimental scattering rate γ in meV by taking the ratio of the experimental resistivity to the calculated value. The average $\gamma = 200$ meV found in frame (c) suggests strong scattering associated with stripe physics. In contrast, ρ_{xy} should be independent of a constant τ , and in Figs. S5(d), 2(b) we find much better agreement with experiment.

In Figs. 2(b) and S5(d) we show two different theoretical calculations, one for $t' = -0.08t$, which captures the steep drop in R_H (Fig. S5(d)), but underestimates the low doping values by a factor of 3, and the other for $t' = -0.12t$, better fitting the low-doping regime and the expected zero-crossing. By substituting a rare earth atom for La, or Ba for Sr, a large variety of LSCO-like compounds can be formed, which have different values for x_{pg} ,¹¹ presumably due to different values of t'/t , as in Fig. S5.

The steep rise of the experimental n_H near $x = 0.2$, followed by a slower variation without clear change of sign at higher doping, is suggestive of significant disorder effects – possibly associated with strong VHS scattering giving

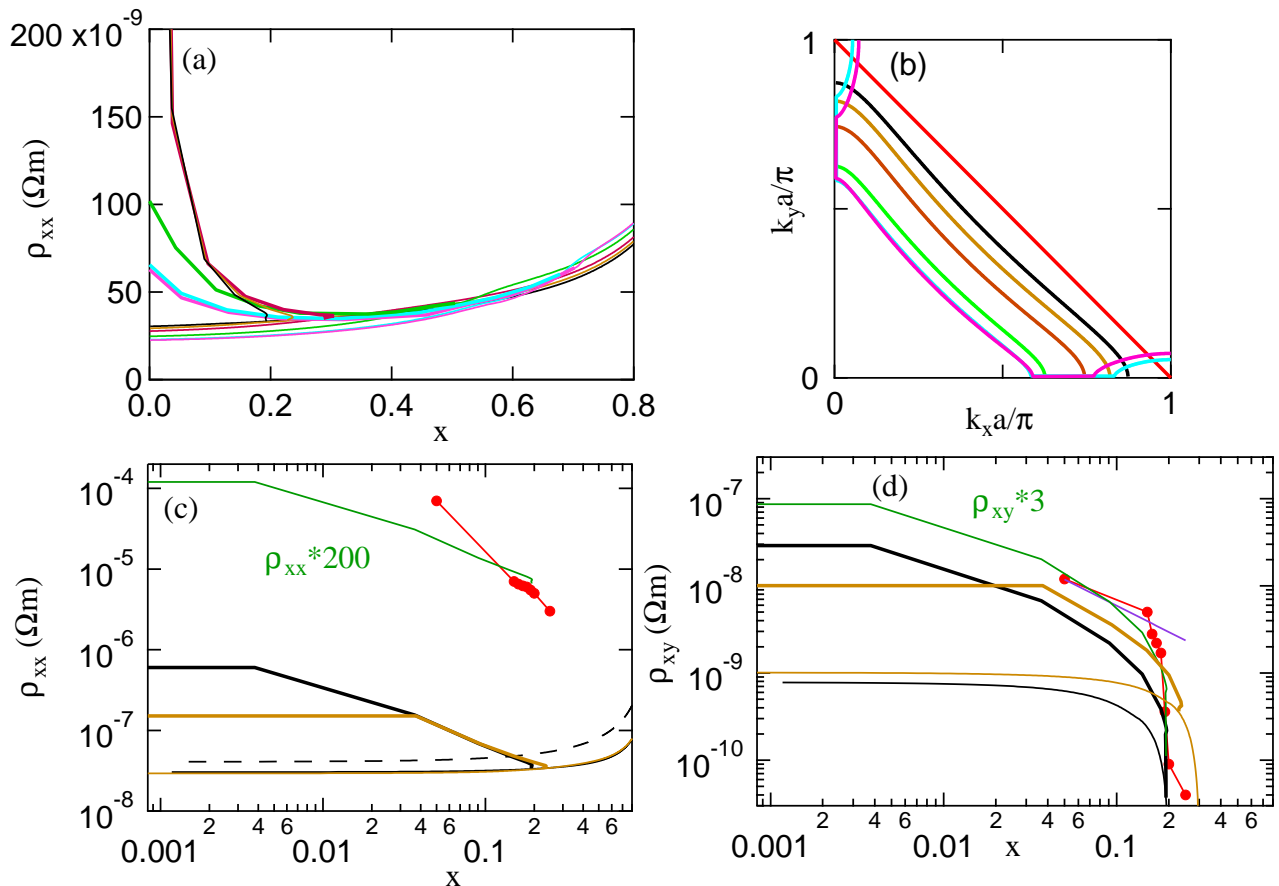


FIG. S5: Low-field Hall effect compared to experiment, showing (a) ρ_{xx} and (b) Fermi surfaces at the Hall zeroes for the same parameter sets as in Fig. S4. Frames (c-d) continue the comparison of theory and experiment for LSCO¹⁰ (red dots) in Fig. 2(b).

rise to a flat-band.^{12,13} In these early experiments sample quality could be an issue, so further experiments at higher doping would be helpful in pinning down the theoretical values.

In passing, we observe that (a), the shift of n_H to the $1+x$ line (violet dashed lines in Figs. 2(b,c)) is not clearly observed in the data, and (b) the NM Hall data show deviations from $1+x$ unless x_{VHS} is quite large, e.g., for Bi2201.

SM-C. DOMAIN WALL PHASE DIAGRAM

To complete this analysis, we briefly discuss how within this model, the domain walls give rise to stripe and CDW phases. We note that phase transitions driven by topological defects can fall outside the standard Landau paradigm, as they can be associated with rearrangements of the defects with no need for nucleation or large entropy change. A well known example is the vortex phase in a type II superconductor in a magnetic field. In a small sample one can calculate the probability for having exactly N vortices, and as the field increases there are transitions from the minimal energy at $N-1$ vortices to N and then to $N+1$ vortices. At fixed vortex number, one can have transitions from hexagonal to square lattices, or to disordered vortices. As a function of sample thickness, there can also be a transition between a type I superconductor, with an intermediate phase consisting of a mixture of finite magnetic and superconducting domains¹⁴, to a type II superconducting film, where the magnetic domains shrink to point vortices.¹⁵

First-principles calculations find stripe phases consistent with hole-doped domain walls in YBCO7⁴, with pre-stripe phases consisting of uncharged antiphase domain walls in YBCO6. In YBCO6 the wall spacing is controlled by repulsion – the walls stay as far apart as possible – similar to the flux lattice in a type II superconductor. In contrast,

in YBCO7, the charge stripe energy oscillates between even and odd periodicities P_c (when measured in terms of the number of Cu atoms between charge stripes), with a minimum energy at $P_c = 4$, consistent with experiment and with fermi surface nesting. We have hypothesized that repulsive stripes evolve into a CDW phase at the Mott-Slater transition, when Fermi surface nesting starts to control the stripe spacing.

SM-C.1. Data used to construct phase diagram

In more detail, Fig. 3(a) sketches the phase diagram found for YBCO in Ref. 16, with three transitions inside the pseudogap detected in Hall effect studies, at T_H , T_{max} , and T_0 (the termination of T_H near $x = 0.16$ is further discussed in Ref. 17). Figure 3 includes superconducting (green lines) and STM data (blue symbols), where we use the following procedure to convert the STM gaps Δ to equivalent onset temperatures. The superconducting gaps have been well studied, and satisfy the relation

$$2\Delta = Xk_B T_c. \quad (\text{S3})$$

For $\text{Bi}_2\text{Sr}_2\text{Ca}_0\text{Cu}_1\text{O}_6$ (Bi2201), $X = 12.4^{18}$, while for Bi2212 $X = 10^{19}$, with weak doping dependence. We assume all STM gap data can be converted to temperatures by the same factor X .

SM-C.2. Quantum oscillations and electron fermi surfaces

We begin our analysis with the two features that seem to be related to the appearance of an electron pocket in the Fermi surface – T_{max} , defined as the temperature of the peak in the Hall coefficient R_H , would indicate the temperature at which the electron pocket first appears, while T_0 , where $R_H = 0$, would be the temperature at which the electron pocket begins to dominate the Hall effect.

Such a pocket suggests the existence of a new phase distinct from the AFM and NM phases, and was soon associated with quantum oscillation (QO) evidence for a CDW phase with very small electron pockets in YBCO. This QO phase has been modeled as a phase of crossed $P_c = 4$ stripes, which reproduces an electron pocket fermi surface of the correct area.²⁰ Consistent with this picture, STM studies²¹ find a crossover (black vertical line in Fig. 3(a)) from commensurate $P_c = 4$ stripes (blue squares labelled T_C) to incommensurate stripes (blue diamonds labelled T_I). The near coincidence of T_{max} and T_C in Fig. 3(a) strongly suggests that both are describing the same stripe phase as the QO studies.

Thus, the phase diagram of YBCO seems to be dominated by a single $P_c = 4$ stripe phase which extends from $x = 0.08$ to $x = 0.18$ – the range over which the electron pocket QO is observed.²² The problem with this electron pocket is that its Fermi surface area changes by only 20% over the full range of doping and temperature.²² This is not what one would expect from a uniform CDW phase, where the Peierls distortion⁴ would modulate the electronic band structure, and doping would cause the bands to fill and fermi surface areas to evolve smoothly, in order to satisfy Luttinger’s theorem.

We propose that the most likely explanation for a doping-independent fermi surface area is in terms of the patch maps seen in scanning tunneling microscopy (STM).²³ Each patch is on average about 3 nm across and has a well defined hole content^{21,24} associated with the local oxygen doping.²⁵ Of all of the stripe structures, only one has a small enough unit cell to fit within the coherence region of a patch. The doping dependence is therefore associated with percolation across patches, and the peak in T_{max} identifies the doping of that particular patch, $x_{QO} \sim 1/8$, where the population is largest. This same stripe, with charge periodicity $P_c = 4$ Cu was found to be the ground state for YBCO7⁴.

For qualitative purposes, one can introduce a simplified percolation model with only three phases, $x_0 = 0$ (corresponding to doping on the magnetic stripes), $x_1 = 0.25$ (on the charged stripes) and $x_{QO} = (x_0 + x_1)/2 = 0.125$ for our stripe phase. Then 2D percolation of the stripe phase would occur when the stripe phase population falls to 50% of the total, or at $(x_0 + x_{QO})/2 = 0.0625$ and $(x_1 + x_{QO})/2 = 0.1875$, close to the experimental range²². Moreover, hopping on the percolation backbone near the limits of percolation could explain the observed effective mass divergence.

In Fig. 3(b) we plot the ratio T_{max}/T_H (red line), and take it as an estimate of the fraction of the sample in the QO-phase, f_{QO} . Note that at x_{QO} , this fraction rises to 84%. The figure includes similar data for the T_C and T_I lines found in Bi2201 (blue symbols); to find the latter we assumed that the total number of domain walls is given by the linear extrapolation of T_H to higher doping.

Is the present model self-consistent? Are the patches large enough to contain the observed QO orbital? If we identify the QO phase with the $P_c = 4$ stripe phase, then since the Cu-Cu separation is about 0.4nm in all cuprates, this

charge periodicity corresponds to 1.6nm, with the magnetic periodicity twice as large, 3.2nm. Thus a 3nm diameter gap patch could approximately hold one 2D magnetic unit cell (the magnetic periodicity is $P_m = 8$), or 4 2D charge cells, or a corresponding stack of 1D stripe cells, and macroscopic effects would have to be associated with percolation of many patches. The tight fit of the magnetic cell might explain why the charge stripe order tends to appear at higher temperatures than the magnetic stripe order²⁶. The largest QO one could observe is limited to the superlattice Brillouin zone area, corresponding to an electron density 0.0625 per planar Cu for a 2D charge cell or 0.0156 for the magnetic cell – the experimental QO Fermi surface accounts for a density ~ 0.04 per Cu.

SM-C.3. T_H and the loss of domain walls

If T^* is the onset of short-range AFM order, as we propose, then T_H has a natural interpretation as the Ising- $X - Y$ transition, where domain walls are the allowed topological defect only below $T = T_H$. As the AFM phase approaches the critical doping from below, the correlation length divergence signals the broadening of the domain walls. When the walls get broad enough, the system will transform from the Ising to an X-Y or Heisenberg model, and the walls will be destabilized. In this range any signal of a CDW phase is lost. This is consistent with a recent proposal that critical fluctuations of the pseudogap melt the charge order.²⁷ The Ising-XY transition was directly observed in early experiments on cuprates²⁸. More recently similar results were found in a very different material, the heavy-fermion triplet-superconductor UTe₂.²⁹

SM-C.4. Further evidence for the Mott-Slater transition

As noted in the main text, at a doping between 0.14 and 0.16, T_H , T_0 , T_{max} , and T_C all terminate discontinuously. The latter three are all associated with $P_c = 4$ stripes and were discussed in the main text. [See also Ref. 30.] The reduction of correlation length across the transition translates to discontinuously smaller gaps on the Slater side. Note that the reduced correlation length may have caused the authors of Ref. 21 to identify x_{CI} with the transition from small to large Fermi surface, which is inconsistent with the presence of an ICDW, which must also gap the Fermi surface.

However, within our picture T_H is associated with all domain walls, so the cutoff at x_{CI} must be a property of the underlying AFM order – e.g., the abrupt drop in correlation length at the Mott-Slater transition³¹, thus offering an independent confirmation for this transition.

We note several additional points about Fig. 4. First, the distinction between dressed x_{VHS} and bare x_{VHS0} is in good semiquantitative agreement with the splitting between the NM VHS and the AFM VHS in the LHB, Fig. 1(b). One difference is that in the pure Hubbard model the VHS is at the band top, so x_{VHS} should extrapolate to 0^+ as $x \rightarrow 0$. However, a small broadening of the VHS would shift the peak to finite doping, and due to the strong divergence of the DOS, a shift to $x \sim 0.11$ would not be surprising.

A similar commensurate Mott phase was found in the 3D Hubbard model (here with $q = (\pi, \pi, \pi)$), which crossed over to a weaker incommensurate phase above a critical doping³².

Ref. 33 did not provide any estimate of t' . To map their data onto Fig. 4, we assumed that the ARPES estimate of x_{VHS} is essentially x_{VHS0} and plotted the data at the appropriate t' . Then Fig. S6 can be used to convert x_{VHS0} to t' , both for the data of Refs 34–36, for which $t'' = 0$ (dark red diamonds), and for the parameters of the PA model, with $t'' = -t'/2$ (violet diamonds). This translates into experimental³³ estimates $t'_{PA} = -0.11$ (LSCO), -0.133 (Nd-substituted LSCO), and -0.23 (Bi2201), in good agreement with other estimates.

SM-C.5. Implications for superconductivity

One implication of the above result is that optimal superconductivity arises very close to the C-I transition, where strongly-correlated Mott states and metallic Slater states coexist. Such a regime has been proposed to be favorable for exotic superconductivity, either because the superconductivity can control the balance between the two competing phases³¹, or because of an exotic pairing mechanism.^{37,38} In this case, the metallic domains would provide mobile carriers while the Mott phase would supply the pairing fluctuations. Notably, experimental evidence for just such a nanoscale phase separation has been found recently^{39,40}.

The STM results, Fig. 3(a), provide some insight into why the superconducting T_c of Bi2201 is so low. The large ratio of Δ_s to T_c is characteristic of what McMillan called strongly-coupled CDWs, driven by phonon entropy.⁴¹ The fact that T_c approximately scales with T_I as a function of doping suggests that superconductivity arises in the ICDW phase – that is, it represents a form of pair density wave.^{42,43} As such, the phononic entropy that reduces T_I will

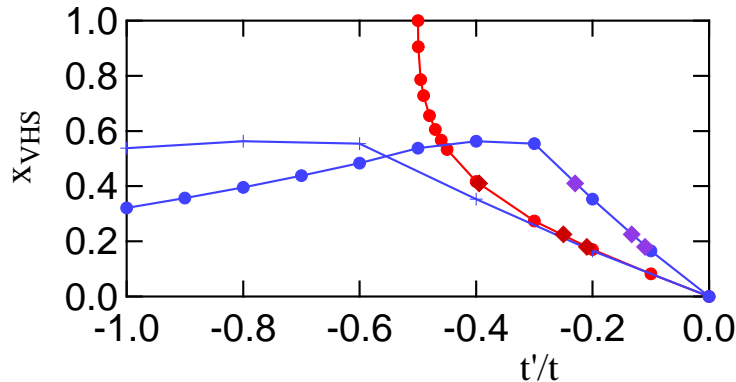


FIG. S6: VHS doping x_{VHS} in the $t - t' - t''$ model for $t''/t' = 0$ (red dots) and -0.5 (blue dots). Dark red and violet diamonds represent t'/t for the data of Ref. 33 within the corresponding models. Note that at low doping t' for $t'' = -0.5t'$ is approximately half t' for $t'' = 0$ (blue + signs).

also have a strong effect on T_c . The Bi2201 superconducting phase diagram should be contrasted with the so-called trisected dome¹⁹ found by ARPES in Bi2212, with the corresponding T_c given by the dark green line in Fig. 3(a). The profound difference between Bi2201 and Bi2212 in their superconducting properties has long been known, but the present results suggest an underlying physical reason. In the competition between AFM and CDW order, the superconductivity ‘lives’ on the AFM phase in Bi2212, but on the CDW phase in Bi2201. Note that for both Bi compounds the superconducting dome terminates near x_{pg} . LSCO resembles Bi2201, in that superconducting and stripe order disappear at the same doping,^{44,45} even when Fe-doped⁴⁶ ($x_c = 0.28$). Note that both LSCO and Bi2201 have anomalously small superconducting T_c s.

SM-D. A PRIMER ON NANOSCALE PHASE SEPARATION

SM-D.1. Binary alloys

The phase diagrams of binary alloys $A_{1-x}B_x$ have been well studied. Typically, commensurate phases $A_N B_{N'}$, where N and N' are integers, have free energy minima in a narrow doping range, and the phase diagram consists of a few commensurate phases separated by two-phase mixtures which are controlled by tie-lines – straight lines drawn tangent to two adjacent free energy curves. If the tie-line lies at lower energy than any other free energy curve, then over that range of doping the system is a two phase mixture, with the relative proportions controlled by the tie line. If one phase has a particularly narrow width of the free energy curve about its minimum, then the phase is sensitive to thermal or impurity disorder, which smear the phase boundary and make its minimum more shallow in energy – when this minimum rises above the tie line for two neighboring phases, that phase becomes unstable.

Something similar should happen with electronic phases inside a single crystal, with one important difference: an electron gas is charged, so if it wants to phase separate, the large Coulomb cost will make macroscopic phase separation impossible. The solution is to make the domain size very small, hence *nanoscale phase separation* (NPS). Seen from a small distance the NPS region looks charge neutral, and most of the Coulomb energy cost is recovered.

SM-D.2. Electronic phases

Now that the principle behind NPS is understood, we look briefly about how it might play out in a few well-known cases, before returning to the cuprates.

SM-D.3. Case studies

1. Electron-hole droplets

First, we look at a case where NPS is unnecessary, electron-hole droplets in photoexcited semiconductors. The droplets consist of a liquid of excitons, but at such high density that the binding of individual excitons is lost, leaving behind a neutral liquid of electrons and holes. Since the liquid is neutral, the sample phase separates into a mixture of droplets and background semiconductor with a low-density exciton gas.⁴⁷ With no Coulomb penalty the droplets can grow to macroscopic sizes.⁴⁸

2. Superconductors in and out of a magnetic field

One of the best known examples of NPS involves magnetism, not charge, and the issues are somewhat different. A type I superconductor tries to expel all magnetic flux, and it is often said that either the superconducting or magnetic phase must win out, with a discontinuous transition between them. But for finite-sized samples there is another option – an intermediate phase which is a two-phase mixture of macroscopic magnetic or superconducting domains. The problem here is that when the magnetic flux leaves the sample, it causes a bunching up of flux lines outside the sample, which reduces the stabilization energy of the intermediate phase, and the problem gets worse as the sample gets thinner. The solution should be obvious by now. Make the magnetic domains smaller, and the bunching outside the sample is reduced. Ultimately the sample undergoes a type I to type II transition, and the field of the resulting vortex lattice produces essentially no bunching of fields.¹⁵

3. Quantum Hall states

The possibility of phase separation in the quantum Hall effect was raised by a result of Prange.⁴⁹ He showed that if a sample was quantized on a Hall plateau, and you cut arbitrary holes in the sample, it would remain quantized as long as the boundary of the sample is preserved. This leads to a model of the transition between adjacent integer plateaus as a percolation transition between domains on adjacent plateaus. The problem in this and other electronic phases is to determine whether the NPS is intrinsic (filled Landau levels have minima in the free energy)^{50,51} or extrinsic (electrons are naturally attracted to impurity clusters, or more generally to minima in the potential landscape), and theories based on both possibilities have been presented. In the latter case, an analogy to a landscape with varying water level has been adduced, where the landscape evolves from a large land mass with a variety of lakes to a large sea with a variety of islands. The intrinsic case has the advantage of a ready connection to the fractional Hall effect: if filled Landau levels are states of low free energy, fractionally filled levels can have similar properties, but with extremely delicate free energy minima, readily disrupted by thermal or impurity disorder. Thus, as samples are made cleaner or taken to lower temperatures, these fractional minima become sharper and deeper, until they can cross the tie-lines between adjacent integer minima.

SM-D.4. Applications to cuprates

Mott believed that the Mott transition must be first order, and almost from the start the role of NPS in cuprate physics was proposed,⁵² and there are now many articles and conference proceedings devoted to the topic.^{53–55} Here we briefly note a few points relevant to the present paper. (1) While in macroscopic phase separations, the domains of each phase are so large that the properties of one phase are almost unaffected by the properties of the other, this is not expected to be the case for NPS. Thus, when La_2CuO_4 is doped with oxygen interstitials, the added oxygen remains mobile below room temperature. Here, a macroscopic phase separation is found, with one phase at optimal doping, the other in a Neel phase with T_N consistent with the undoped phase.^{56–58} (Recall that in LSCO, optimal doping falls close to x_{VHS} .) Moreover, in the doped phase T_c is actually higher than found in La-cuprates prepared by different doping. Other dopants in the LSCO family are immobile, and lead to a T_c that varies smoothly with doping, with clear evidence of stripes, but no sign of macroscopic phase separation.

(2) Since the hole excess on the charged stripes does not change much with sample doping, the stripes may themselves be an (intrinsic) form of NPS. In contrast, oxygen dopant clusters give rise to an extrinsic form of NPS, the gap maps. The distinction is that oxygen clusters can lead to pinning at any doping, depending on the dopant configuration, while intrinsic NPS tends to be a mix of two particular dopings, as in binary alloys. While these special dopings

were initially taken as the undoped insulator, $x = 0$, and x_{VHS} , more recently there have been suggestions of special phases at $x = 1/8$ and possibly other values.⁵⁹

(3) We summarize some recent results on NPS. As already noted, SCAN results suggest that near optimal doping YBCO is a fluctuating mixture of stripe-like phases⁴, and that this may be a common motif in cuprates⁶⁰ and other correlated materials^{61–66}. The small correlation length limit of this model is consistent with the SQS model⁶⁷.

The Mott-Slater crossover is a high entropy phase with very short correlation length, suggestive of a spin liquid phase, which could be avoided by NPS.³¹ Notably, in a recent series of papers, it was demonstrated that superconducting fluctuations in most cuprates above T_c cannot be explained by Ginzburg-Landau physics, but are consistent with a *universal* percolative superconductivity.^{39,40,68} It was proposed⁶⁹ that the percolation arises due to pseudogap-related inhomogeneity of the ‘normal’ state. This is consistent with earlier proposals for optimizing superconductivity^{37,38}, and with the fact that optimal superconductivity falls close to the Mott-Slater transition.³¹

With this background, we look at the results of the current investigation. The QO phase seems to be associated with a stripe phase near 1/8th doping, which may be the dominant phase over a range of dopings. Its transition temperature seems to vary systematically with doping, as found for the superconducting T_c , with an ‘optimal doping’ at $x = 1/8$. The second example is the broadened AFM VHS peak we find at the pseudogap termination. As discussed in SM-A.1, this could be associated with gap map broadening over a large doping range about x_{pg} . Note that while in a uniform system the AFM phase should terminate at x_{pg} , persistence of gap maps into the overdoped regime could produce a residue of AFM order at higher doping.⁷⁰

SM-E. NOTES ON THE DISCUSSION SECTION

SM-E.1. 3 VHSs

A surprising property of cuprates is that ARPES seems to see the bare fermi surface even in undoped samples.⁷¹ Actually, this is not a real fermi surface, since its intensity is quite weak, but its origin is not clear. This origin could be trivial (a diffraction effect), interesting (a competing phase), or exotic (a non-fermi liquid). Below, these choices are briefly discussed.

When a single crystal is cooled across an electronic phase transition, grains of the electronic phase nucleate independently throughout the crystal and grow together. These electronic grains are unique, in that they are all epitaxial with the underlying crystal, and so can only differ by how they decorate a unit cell or by the local doping. This gives rise to a JPEG-effect, where masking off just one kind of patch leads to an image of a single crystal of fixed doping, but with reduced resolution, so that, e.g., an underlying Fermi surface can be extracted which can be used to find the gap as a function of doping, all in a single sample^{21,24}. Since ARPES samples a large area which cannot be masked, it also gives a fermi surface image, which is a broadened average of the STM fermi surfaces. Surprisingly, for both STM and ARPES, only the NM fermi surface is seen. This could be a diffraction effect, since even the masked STM images contain a random array of all possible decorations of the unit cell. For example, the $P_c = 4$ 1D stripe contains $8 \times 2 = 16$ atoms in the magnetic unit cell, and hence 16 inequivalent ways to decorate the unit cell. Thus while all cells share the same NM charge distribution, the superlattice distribution is a random mix of 16 patterns, which will tend to wash out any trace of the superlattice fermi surfaces.

Alternatively, the ghost fermi surface could be caused by a competing order – e.g., a manifestation of a zero crossing of the electronic Green’s function, which in turn is caused by a divergence of the electronic self energy, $\Sigma^{AF}(\omega, k) \sim \Delta^{AF2}/(\omega - \epsilon_{k+Q})$, where $Qa = (\pi, \pi)$.⁷² The apparent fermi surface is associated with a broad (in ω) tail in the spectral function crossing the fermi level. A signature of this effect is that the ARPES intensity is very small, decreasing as the gap Δ^{AF} increases. Superconductivity causes similar effects, and it has been proposed that the Fermi arc is mainly associated with this zero-crossing.⁷³

This zero-crossing is useful in that it gives direct access to the bare VHS and x_{VHS0} . At the same time, it greatly complicates observation of the small fermi surface and the crossover to a large fermi surface, particularly since its intensity increases as the gap collapse is approached. Some studies find that the zero crossing exists only up to the AFM zone boundary (see Ref. 72), giving access to the crossover to a large fermi surface outside the first AFM Brillouin zone.^{74,75} Recent improvements in technique allow absolute measurements in ARPES intensity, showing how the ghost intensity increases as the pseudogap collapse is approached⁷⁶.

Finally, we note that Yang, Rice, and Zhang were able to explain the STM fermi surfaces by modifying the Green’s

function zero crossing⁷⁵, but only at the cost of violating Luttinger’s theorem.

-
- ¹ Das, T. Markiewicz, R.S. and Bansil, A., Intermediate coupling model of the cuprates, *Advances in Physics* 63, 151-266 (2014).
 - ² J. M. Tranquada, “Neutron scattering studies of antiferromagnetic correlations in cuprates,” in *Handbook of High Temperature Superconductivity*, pp. 257–298, Springer, Berlin, 2007.
 - ³ Kanun Pokharel, Christopher Lane, James W. Furness, Ruiqi Zhang, Jinliang Ning, Bernardo Barbiellini, Robert S. Markiewicz, Yubo Zhang, Arun Bansil, Jianwei Sun, Sensitivity of the electronic and magnetic structures of cuprate superconductors to density functional approximations, arXiv:2004.08047.
 - ⁴ Yubo Zhang, Christopher Lane, James W. Furness, Bernardo Barbiellini, John P. Perdew, Robert S. Markiewicz, Arun Bansil, and Jianwei Sun, “Landscape of competing stripe and magnetic phases in cuprates”, *PNAS* 117, 68 (2019).
 - ⁵ S. Ono, S. Komiyama, and Y. Ando, Strong charge fluctuations manifested in the high-temperature Hall coefficient of high- T_c cuprates *Phys. Rev. B* 75, 024515 (2007).
 - ⁶ Robert S. Markiewicz, Yubo Zhang, Christopher Lane, Bernardo Barbiellini, Jianwei Sun, and Arun Bansil, A first-principles-based study of the thermodynamics of competing low-energy states in correlated materials: Example of cuprates, arXiv:1906.05217.
 - ⁷ M. Horio, K. Hauser, Y. Sassa, Z. Mingazheva, D. Sutter, K. Kramer, A. Cook, E. Nocerino, O. K. Forslund, O. Tjernberg, M. Kobayashi, A. Chikina, N. B. M. Schröter, J. A. Krieger, T. Schmitt, V. N. Strocov, S. Pyon, T. Takayama, H. Takagi, O. J. Lipscombe, S. M. Hayden, M. Ishikado, H. Eisaki, T. Neupert, M. Mansson, [xxx] Three-Dimensional Fermi Surface of Overdoped La-Based Cuprates, *Phys. Rev. Lett.* 121, 077004 (2018).
 - ⁸ Q. Li, M. Hücker, G. D. Gu, A. M. Tsvetlik, and J. M. Tranquada, Two-Dimensional Superconducting Fluctuations in Stripe-Ordered $\text{La}_{1.875}\text{Ba}_{0.125}\text{CuO}_4$, *Phys. Rev. Lett.* 99, 067001 (2007).
 - ⁹ V. P. S. Awana, L. Menon, and S. K. Malik, Synthesis and magnetism of $\text{Bi}_2\text{Sr}_2\text{RCu}_2\text{O}_{8+\delta}$ (R=Y, Pr, and Tb) systems, *Phys. Rev. B* 51, 9379 (1995).
 - ¹⁰ N. P. Ong, Z. Z. Wang, J. Clayhold, J. M. Tarascon, L. H. Greene, and W. R. McKinnon, Hall effect of $\text{La}_{2-x}\text{Sr}_x\text{CuO}_4$: Implications for the electronic structure in the normal state, *Phys. Rev. B* 35, 8807(R) (1987).
 - ¹¹ B. Michon, C. Girod, S. Badoux, J. Kamark, Q. Ma, M. Dragomir, H. A. Dabkowska, B. D. Gaulin, J. -S. Zhou, S. Pyon, T. Takayama, H. Takagi, S. Verret, N. Doiron-Leyraud, C. Marcenat, L. Taillefer, and T. Klein, Thermodynamic signatures of quantum criticality in cuprates, *Nature* 567, 218 (2019).
 - ¹² Elbio Dagotto, Alexander Nazarenko, and Adriana Moreo, Flat quasiparticle dispersion in the 2D t - J model, *Phys. Rev. Lett.* 73, 728 (1995).
 - ¹³ N. Bulut, D.J. Scalapino, and S.R. White, Quasiparticle dispersion in the cuprate superconductors and the two-dimensional Hubbard model *Phys. Rev. B* 50, 7215 (1994).
 - ¹⁴ R.P. Huebener, *Magnetic Flux Structures in Superconductors*, (Springer-Verlag, Berlin, 1979).
 - ¹⁵ R.N. Goren and M. Tinkham, Patterns of magnetic flux penetration in superconducting films, *J. Low-Temp. Phys.* 5, 465 (1971).
 - ¹⁶ David LeBoeuf, Nicolas Doiron-Leyraud, B. Vignolle, Mike Sutherland, B. J. Ramshaw, J. Levallois, R. Daou, Francis Laliberté, Olivier Cyr-Choinière, Johan Chang, Y. J. Jo, L. Balicas, Ruixing Liang, D. A. Bonn, W. N. Hardy, Cyril Proust, and Louis Taillefer, “Lifshitz critical point in the cuprate superconductor $\text{YBa}_2\text{Cu}_3\text{O}_y$ from high-field Hall effect measurements”, *Phys. Rev. B* 83, 054506 (2011).
 - ¹⁷ C. Girod, D. LeBoeuf, A. Demuer, G. Seyfarth, S. Imajo, K. Kindo, Y. Kohama, M. Lizaire, A. Legros, A. Gourgout, H. Takagi, T. Kurosawa, M. Oda, N. Momono, J. Chang, S. Ono, G. -q. Zheng, C. Marcenat, L. Taillefer, and T. Klein, $\text{Bi}_{2+y}\text{Sr}_{2-x-y}\text{La}_x\text{CuO}_{6+\delta}$ near the critical point of the pseudogap phase, *Phys. Rev. B* 103, 214506 (2021).
 - ¹⁸ M.C. Boyer, W.D. Wise, K. Chatterjee, M. Yi, T. Kondo, T. Takeuchi, H. Ikuta, and E.W. Hudson, Imaging the two gaps of the high-temperature superconductor $\text{Bi}_2\text{Sr}_2\text{CuO}_{6+x}$, *Nature Physics* 3, 802 (2007).
 - ¹⁹ I. M. Vishik, M Hashimoto, R.-H. He, W. S. Lee, F. Schmitt, D. H. Lu, R. G. Moore, C. Zhang, W. Meevasana, T. Sasagawa, S. Uchida, K. Fujita, S. Ishida, M. Ishikado, Y. Yoshida, H. Eisaki, Z. Hussain, T. P. Devereaux, and Z.-X. Shen, Phase competition in trisected superconducting dome, *PNAS* 109, 18332 (2012).
 - ²⁰ N. Harrison and S.E. Sebastian, Protected Nodal Electron Pocket from Multiple-Q Ordering in Underdoped High Temperature Superconductors, *Physical Review Letters* 106, 226402 (2011).
 - ²¹ Tatiana A. Webb, Michael C. Boyer, Yi Yin, Debanjan Chowdhury, Yang He, Takeshi Kondo, T. Takeuchi, H. Ikuta, Eric W. Hudson, Jennifer E. Hoffman, Mohammad and H. Hamidian, Density wave probes cuprate quantum phase transition, *Phys. Rev. X* 9, 021021 (2019).
 - ²² B.J. Ramshaw, S.E. Sebastian, R.D. McDonald, J. Day, B.S. Tan, Z. Zhu, J.B. Betts, R. Liang, D.A. Bonn, W.N. Hardy, and N. Harrison, Quasiparticle mass enhancement approaching optimal doping in a high- T_c superconductor, *Science* 348, 317 (2015).
 - ²³ J. W. Alldredge, Jinho Lee, K. McElroy, M. Wang, K. Fujita, Y. Kohsaka, C. Taylor, H. Eisaki, S. Uchida, P. J. Hirschfeld, and J. C. Davis, Evolution of the electronic excitation spectrum with strongly diminishing hole-density in superconducting $\text{Bi}_2\text{Sr}_2\text{CaCu}_2\text{O}_{8+\delta}$, *Nature Physics*, 4 319 (2008).
 - ²⁴ W. D. Wise, Kamalesh Chatterjee, M. C. Boyer, Takeshi Kondo, T. Takeuchi, H. Ikuta, Zhijun Xu, Jinsheng Wen, G. D. Gu,

- Yayu Wang and E. W. Hudson, Imaging nanoscale Fermi-surface variations in an inhomogeneous superconductor, *Nature Physics* 5, 213 (2009).
- 25 I. Zeljkovic, Z. Xu, J. Wen, G. Gu, R.S. Markiewicz, and J.E. Hoffman, Imaging the impact of single oxygen atoms on superconducting $\text{Bi}(2+y)\text{Sr}(2-y)\text{CaCu}_2\text{O}(8+x)$, *Science* 337, 320 (2012).
 - 26 M. Huecker, M. v. Zimmermann, G. D. Gu, Z. J. Xu, J. S. Wen, Guangyong Xu, H. J. Kang, A. Zheludev, and J. M. Tranquada, Stripe order in superconducting $\text{La}_{2-x}\text{Ba}_x\text{CuO}_4$ for $0.095 \leq x \leq 0.155$, *Phys. Rev. B* 83, 104506 (2011).
 - 27 W. S. Lee, K. J. Zhou, M. Hepting, J. Li, A. Nag, A. C. Walters, M. Garcia-Fernandez, H. Robarts, M. Hashimoto, H. Lu, B. Nosarzewski, D. Song, H. Eisaki, Z. X. Shen, B. Moritz, J. Zaanen, and T. P. Devereaux, Spectroscopic Evidence for Charge Order Melting via Quantum Fluctuations in a Cuprate, arXiv:2007.02464.
 - 28 Tineke Thio, T. R. Thurston, N. W. Preyer, P. J. Picone, M. A. Kastner, H. P. Jenssen, D. R. Gabbe, C. Y. Chen, R. J. Birgeneau, and Amnon Aharony, Antisymmetric exchange and its influence on the magnetic structure and conductivity of La_2CuO_4 , *Phys. Rev. B* 38, 905(R) (1988).
 - 29 Dexin Li, Ai Nakamura, Fuminori Honda, Yoshiki J. Sato, Yoshiya Homma, Yusei Shimizu, Jun Ishizuka, Youichi Yanase, Georg Knebel, Jacques Flouquet, and Dai Aoki, Magnetic Properties under Pressure in Novel Spin-Triplet Superconductor UTe_2 , *J. Phys. Soc. Jpn.* 90, 073703 (2021).
 - 30 A. Mesaros, K. Fujita, S. D. Edkins, M. H. Hamidian, H. Eisaki, S. Uchida, J. C. Séamus Davis, M. J. Lawler, and Eun-Ah Kim, Commensurate $4a_0$ period Charge Density Modulations throughout the $\text{Bi}_2\text{Sr}_2\text{CaCu}_2\text{O}_{8+x}$ Pseudogap Regime, *Proc. Natl. Acad. Sci. U.S.A.*, 113, 12661 (2016).
 - 31 R.S. Markiewicz, I.G. Buda, P. Mistark, and A. Bansil, Entropic origin of pseudogap physics and a Mott-Slater transition in cuprates *Nature Scientific Reports* 7, 44008 (2017).
 - 32 T. Schäfer, A.A. Katanin, K. Held, and A. Toschi, Interplay of Correlations and Kohn Anomalies in Three Dimensions: Quantum Criticality with a Twist *Phys. Rev. Lett.* 119, 046402 (2017).
 - 33 N. Doiron-Leyraud, O. Cyr-Choinière, S. Badoux, A. Ataei, C. Collignon, A. Gourgout, S. Dufour-Beauséjour, F.F. Tafti, F. Laliberté, M.-E. Boulanger, M. Matusiak, D. Graf, M. Kim, J.-S. Zhou, N. Momono, T. Kurosawa, H. Takagi, Louis Taillefer Pseudogap phase of cuprate superconductors confined by Fermi surface topology *Nature Communications* 8, 2044 (2017)
 - 34 Wei Wu, Mathias S. Scheurer, Shubhayu Chatterjee, Subir Sachdev, Antoine Georges, and Michel Ferrero, Pseudogap and Fermi surface topology in the two-dimensional Hubbard model, *Phys. Rev. X* 8, 021048 (2018).
 - 35 Braganca, H. Sakai, S. Aguiar, M.C.O. and Civelli, M. Correlation-driven Lifshitz transition at the emergence of the pseudogap phase in the two-dimensional Hubbard model *Phys. Rev. Lett.* 120, 067002 (2018).
 - 36 Wei Wu, Xiang Wang, and André-Marie Tremblay, Non-Fermi liquid phase and linear-in-temperature scattering rate in overdoped two dimensional Hubbard model, *PNAS* 113, e2115819119 (2022) (arXiv:2109.02635).
 - 37 W.A. Little, Possibility of Synthesizing an Organic Superconductor. *Phys. Rev.* A134, 1416 (1964).
 - 38 A. Allender, J.W. Bray, and J. Bardeen, Theory of fluctuation superconductivity from electron-phonon interactions in pseudo-one-dimensional systems *Phys. Rev.* B9, 119 (1974).
 - 39 D. Pelc, M. Vučković, M. Grbić, M. Požek, G. Yu, T. Sasagawa, T.M. Greven, and N. Barišić, Emergence of superconductivity in the cuprates via a universal percolation process, *Nature Communications* 9, 4327 (2018).
 - 40 P. Popčević, D. Pelc, Y. Tang, K. Velebit, Z. Anderson, V. Nagarajan, G. Yu, M. Požek, N. Barišić, and M. Greven, Percolative nature of the dc paraconductivity in the cuprate superconductors *npj Quantum Materials* 3, 42 (2018).
 - 41 W.L. McMillan, Microscopic model of charge-density waves in 2H-TaSe₂. *Phys. Rev.* B16, 643 (1977).
 - 42 D. Chakraborty, M. Grandadam, M. H. Hamidian, J. C. S. Davis, Y. Sidis, and C. Pépin, Fractionalized pair density wave in the pseudo-gap phase of cuprate superconductors, *Phys. Rev. B* 100, 224511 (2019).
 - 43 P. M. Lozano, Tianhao Ren, G. D. Gu, A. M. Tsvelik, J. M. Tranquada, and Qiang Li, Phase-sensitive evidence of pair-density-wave order in a cuprate, arXiv:2110.05513.
 - 44 S. Wakimoto, K. Yamada, J. M. Tranquada, C. D. Frost, R. J. Birgeneau, and H. Zhang, Disappearance of antiferromagnetic spin excitations in overdoped $\text{La}_{2-x}\text{Sr}_x\text{CuO}_4$, *Phys. Rev. Lett.* 98, 247003 (2007).
 - 45 O.J. Lipscombe, S.M. Hayden, B. Vignolle, D.F. McMorrow, and T.G. Perring, Persistence of high-frequency spin fluctuations in overdoped superconducting $\text{La}_{2-x}\text{Sr}_x\text{CuO}_4$ ($x = 0.22$), *Phys. Rev. Lett.* 99, 067002 (2007).
 - 46 K.M. Suzuki, T. Adachi, H. Sato, I. Watanabe, and Y.I. Koike, Successive magnetic transitions relating to itinerant spins and localized Cu spins in $\text{La}_{2-x}\text{Sr}_x\text{Cu}_{1-y}\text{Fe}_y\text{O}_4$: Possible existence of stripe correlations in the overdoped regime, *Journal of the Physical Society of Japan* 85, 124705 (2016).
 - 47 C.D. Jeffries and L.V. Keldysh, Eds., *Electron-hole droplets in semiconductors*, (Elsevier, Amsterdam, 1983).
 - 48 J.P. Wolfe, R.S. Markiewicz, C. Kittel, and C.D. Jeffries, Observation of Large Long-Lived Electron-Hole Drops in Germanium, *Phys. Rev. Lett.* 34, 275 (1975).
 - 49 Robert Joynt and R. E. Prange, Conditions for the quantum Hall effect, *Phys. Rev. B* 29, 3303 (1984).
 - 50 R. S. Markiewicz, Condon domains in the two-dimensional electron gas. I. Domain-to-vortex transition, *Phys. Rev. B* 34, 4172 (1986).
 - 51 R. S. Markiewicz, Condon domains in the two-dimensional electron gas. II. Charging effects, *Phys. Rev. B* 34, 4177 (1986).
 - 52 R.S. Markiewicz, Spinoidal Decomposition near a Lifshitz Point, *Mod. Phys. Letts.* B1, 187 (1987).
 - 53 R.S. Markiewicz, A survey of the Van Hove scenario for high- T_c superconductivity with special emphasis on pseudogaps and striped phases, *J. Phys. Chem. Sol.* 58, 1179 (1997).
 - 54 K.A. Müller and G. Benedek, Eds. *Phase Separation in Cuprate Superconductors*, (World, Singapore, 1992).
 - 55 E. Sigmund and K.A. Müller, *Phase Separation in Cuprate Superconductors*, (Springer, Berlin, 1994).
 - 56 J.D. Jorgensen, B. Dabrowski, S. Pei, D.G. Hinks, L. Soderholm, B. Morosin, J.E. Schirber, E.L. Venturini and D.S. Ginley,

- Superconducting phase of $\text{La}_2\text{CuO}_{4+\delta}$: A superconducting composition resulting from phase separation, *Phys. Rev. B* 38, 11337 (1988).
- ⁵⁷ See Section 11.1.1 in Ref.53.
- ⁵⁸ Thomas Jarlborg and Antonio Bianconi, Fermi surface reconstruction of superoxygenated La_2CuO_4 superconductors with ordered oxygen interstitials, *Phys. Rev. B* 87, 054514 (2013).
- ⁵⁹ Seiki Komiya, Han-Dong Chen, Shou-Cheng Zhang, and Yoichi Ando, Magic Doping Fractions in High-Temperature Superconductors, *Phys. Rev. Lett.* 94, 207004 (2005).
- ⁶⁰ K. I. Kugel, A. L. Rakhmanov, A. O. Sboychakov, Nicola Poccia, and Antonio Bianconi, Model for phase separation controlled by doping and the internal chemical pressure in different cuprate superconductors, *Phys. Rev. B* 78, 165124 (2008).
- ⁶¹ Christopher Lane, Yubo Zhang, James W. Furness, Robert S. Markiewicz, Bernardo Barbiellini, Jianwei Sun, and Arun Bansil, First-Principles Calculation of Spin and Orbital Contributions to Magnetically Ordered Moments in Sr_2IrO_4 , *Phys. Rev. B* 101, 155110 (2020).
- ⁶² Ruiqi Zhang, Christopher Lane, Bahadur Singh, Johannes Nokelainen, Bernardo Barbiellini, Robert S. Markiewicz, Arun Bansil, and Jianwei Sun, f-electron and magnetic ordering effects in nickelates LaNiO_2 and NdNiO_2 : remarkable role of the cuprate-like $3d_{x^2-y^2}$ band, *Commun. Phys.* 4, 118 (2021).
- ⁶³ Ruiqi Zhang, Bahadur Singh, Christopher Lane, Jamin Kidd, Yubo Zhang, Bernardo Barbiellini, Robert S. Markiewicz, Arun Bansil, and Jianwei Sun, Understanding the Quantum Oscillation Spectrum of Heavy-fermion Compound SmB_6 , arXiv:2003.11052.
- ⁶⁴ A. Ricci, N. Poccia, B. Joseph, D. Innocenti, G. Campi, A. Zozulya, F. Westermeier, A. Schavkan, F. Coneri, A. Bianconi, H. Takeya, Y. Mizuguchi, Y. Takano, T. Mizokawa, M. Sprung, and N. L. Saini, Direct observation of nanoscale interface phase in the superconducting chalcogenide $\text{K}_x\text{Fe}_{2-y}\text{Se}_2$ with intrinsic phase separation, *Phys. Rev. B* 91, 020503(R) (2015).
- ⁶⁵ Yangmu Li, Nader Zaki, Vasile O. Garlea, Andrei T. Savici, David Fobes, Zhijun Xu, Fernando Camino, Cedimir Petrovic, Genda Gu, Peter D. Johnson, John M. Tranquada, and Igor A. Zaliznyak, Magnetic, superconducting, and topological surface states on $\text{Fe}_{1+y}\text{Te}_{1-x}\text{Se}_x$, *Nat. Mater.* 20, 1221 (2021).
- ⁶⁶ L. Simonelli, V. Palmisano, M. Fratini, M. Filippi, P. Parisiades, D. Lampakis, E. Liarokapis, and A. Bianconi, Isotope effect on the E_{2g} phonon and mesoscopic phase separation near the electronic topological transition in $\text{Mg}_{1-x}\text{Al}_x\text{B}_2$, *Phys. Rev. B* 80, 014520 (2009).
- ⁶⁷ Alex Zunger, S.-H. Wei, L. G. Ferreira, and James E. Bernard, Special quasirandom structures, *Phys. Rev. Lett.* 65, 353 (1990).
- ⁶⁸ G. Yu, D.-D. Xia, D. Pelc, R.-H. He, N.-H. Kaneko, T. Sasagawa, Y. Li, X. Zhao, N. Barišić, A. Shekhter, and M. Greven, Universal superconducting precursor in the cuprates *Phys. Rev. B* 98, 161114 (2018).
- ⁶⁹ D. Popčević, P. Yu, G. Požek, M. Greven, and N. Barišić, Unusual behavior of cuprates explained by heterogeneous charge localization, *Science Advances* 5, eaau4538 (2019).
- ⁷⁰ N. E. Hussey, J. Buhot, and S. Licciardello, A Tale of Two Metals: contrasting criticalities in the pnictides and hole-doped cuprates, *Rev. Prog. Phys.* 81, 052501 (2018).
- ⁷¹ S. Sahrakorpi, R. S. Markiewicz, Hsin Lin, M. Lindroos, X. J. Zhou, T. Yoshida, W. L. Yang, T. Kakeshita, H. Eisaki, S. Uchida, Seiki Komiya, Yoichi Ando, F. Zhou, Z. X. Zhao, T. Sasagawa, A. Fujimori, Z. Hussain, Z. -X. Shen, and A. Bansil, Appearance of Universal Metallic Dispersion in a Doped Mott Insulator, *Phys. Rev. B* 78, 104513 (2008).
- ⁷² C. Kusko and R. S. Markiewicz, Remnant Fermi Surfaces in Photoemission, *Phys. Rev. Lett.* 84, 963 (2000).
- ⁷³ T. J. Reber, N. C. Plumb, Z. Sun, Y. Cao, Q. Wang, K. McElroy, H. Iwasawa, M. Arita, J. S. Wen, Z. J. Xu, G. Gu, Y. Yoshida, H. Eisaki, Y. Aiura, and D. S. Dessau, The Origin and Non-quasiparticle Nature of Fermi Arcs in $\text{Bi}_2\text{Sr}_2\text{CaCu}_2\text{O}_{8+\delta}$, *Nature Physics* 8, 606 (2012).
- ⁷⁴ Y. Kohsaka, C. Taylor, P. Wahl, A. Schmidt, Jinhwan Lee, K. Fujita, J. W. Alldredge, K. McElroy, Jinho Lee, H. Eisaki, S. Uchida, D.-H. Lee, and J. C. Davis, How Cooper pairs vanish approaching the Mott insulator in $\text{Bi}_2\text{Sr}_2\text{CaCu}_2\text{O}_{8+\delta}$, *Nature*, 454, 1072 (2008).
- ⁷⁵ Kai-Yu Yang, H. B. Yang, P. D. Johnson, T. M. Rice, and Fu-Chun Zhang, Quasiparticles in the Pseudogap Phase of Underdoped Cuprate, *EPL* 86, 37002 (2009).
- ⁷⁶ Incoherent strange metal sharply bounded by a critical doping in $\text{Bi}2212$, Su-Di Chen, Makoto Hashimoto, Yu He, Dongjoon Song, Ke-Jun Xu, Jun-Feng He, Thomas P. Devereaux, Hiroshi Eisaki, Dong-Hui Lu, Jan Zaanen, and Zhi-Xun Shen, *Science* 366, 1099 (2019).